

# I.FAST

Innovation Fostering in Accelerator Science and Technology

Horizon 2020 Research Infrastructures GA n° 101004730

## DELIVERABLE REPORT

### First 6 GHz cavity coated and characterised

#### DELIVERABLE: D9.3

<b>Document identifier:</b>	IFAST-D9.3
<b>Due date of deliverable:</b>	End of Month 51 (July 2025)
<b>Report release date:</b>	01/08/2025
<b>Work package:</b>	WP9: Innovative superconducting cavities
<b>Lead beneficiary:</b>	STFC
<b>Document status:</b>	Final

#### ABSTRACT

This report is on Deliverable D9.3: First 6 GHz cavity coated and characterised. The Report show the results from the morphological and SC characterisation of planar samples coated with material different from niobium such as Nb<sub>3</sub>Sn, NbTiN and V<sub>3</sub>Si. That results of RF surface resistance on planar samples at 7.8 GHz chocked cavity and on 400 MHz on QPR measurements at 4 K demonstrate that Nb<sub>3</sub>Sn is the most suitable material for cavity coatings.

Then first coated 6 GHz cavity was coated with NbTiN an alternative material to niobium and RF tested. The RF results show low Q and Eacc due to lack of suitable deposition targets with required composition. This work to be continued in the future.

The 6 GHz split cavity was deposited with Nb<sub>3</sub>Sn in planar configuration. The RF test demonstrated that its performance is limited by cavity geometry rather than the quality of the film. The split cavity geometry has been changed to address this feature and future tests are ongoing.

Based on work performed in Task 9.3, the decision for 1.3 GHz cavity coating material and technology was taken to drive a delivery in Task 9.2.

I.FAST Consortium, 2025

For more information on IFAST, its partners and contributors please see <https://ifast-project.eu/>

This project has received funding from the European Union's Horizon 2020 Research and Innovation programme under Grant Agreement No 101004730. IFAST began in May 2021 and will run for 4 years.

### Delivery Slip

	Name	Partner	Date
Authored by	R.Valizadeh, O.Malyshev	UKRI	28/07/2025
	C. Pira	INFN	
	E. Seiler	IEE	
	A. Zubitskii	USI	
Reviewed by	M. Vretenar, L. Celona [on behalf of Steering Committee]	CERN	01/08/2025
Approved by	Steering Committee		01/08/2025

## TABLE OF CONTENTS

<b>1</b>	<b>INTRODUCTION.....</b>	<b>4</b>
<b>2</b>	<b>SUPERCONDUCTING THIN FILMS ON PLANAR SAMPLES.....</b>	<b>5</b>
2.1	Nb <sub>3</sub> Sn ON FLAT SAMPLES.....	5
2.1.1	Optimisation of Nb <sub>3</sub> Sn deposition on Copper using Choke cavity (UKRI).....	5
2.1.2	Optimisation of Nb <sub>3</sub> Sn On Cu, Nb and SAPPHIRE at INFN.....	7
2.1.3	Nb <sub>3</sub> Sn deposition on Silicon at USI.....	9
2.2	NbTiN DEPOSITION.....	9
2.2.1	Deposition of NbTiN on flat sample at USI by DCMS.....	9
2.2.2	NbTiN deposition by HiPIMS (study was carried out by Bharath Reddy Lakki Reddy Venkata).....	12
2.3	V <sub>3</sub> SI DEPOSITION ON FLAT SAMPLE.....	13
2.4	CHARACTERISATION OF FLAT SAMPLES VIA MAGNETIZATION MEASUREMENTS.....	14
<b>3</b>	<b>DEPOSITION ON 6 GHZ COPPER CAVITY.....</b>	<b>17</b>
3.1	NbTiN deposition of 6 GHz closed copper cavity.....	17
3.1.1	Deposition chamber at UKRI.....	17
3.1.2	Deposition chamber at INFN.....	17
3.1.3	SRF measurement facility at INFN.....	19
3.1.4	Deposition parameters and analysis at UKRI.....	20
3.1.5	Split 6 GHz copper cavity.....	23
3.2	SPLIT CAVITIES.....	24
3.2.1	Cavity Tests.....	24
3.2.2	Results.....	24
<b>4</b>	<b>TARGET PRODUCTION AT INFN.....</b>	<b>29</b>
4.1	PROOF OF CONCEPT ON OLD DIPPING SYSTEM.....	29
4.2	NEW DIPPING SYSTEM.....	30
<b>5</b>	<b>CONCLUSIONS AND RELATION TO OTHER IFAST WORK.....</b>	<b>32</b>
5.1	MAIN RESULTS.....	32
5.2	FUTURE PLANS.....	32
<b>6</b>	<b>REFERENCES.....</b>	<b>33</b>

## Executive summary

*Optimisation of deposition parameters and characterisation of superconducting thin film of material other than Nb such as Nb<sub>3</sub>Sn, NbTiN and V<sub>3</sub>Si for 6 GHz cavity deposition, 7.8 GHz choke cavity and quadrupole resonator (QPR).*

*Based on work performed in this task, the decision for 1.3 GHz cavity coating material and technology was taken to drive a delivery in Task 9.2.*

*Copper mock cavities and tubes coated with Nb are also being provided to RTU for post-deposition laser treatment.*

## 1 Introduction

Radio-frequency (RF) cavities play a critical role in accelerating charged particles within particle accelerators, supporting a wide array of applications across science, healthcare, safety, and industry. Currently, RF cavities constructed from superconducting materials such as niobium are considered the most effective option due to niobium's high critical temperature ( $T_c = 9.25$  K), superior superheating magnetic field ( $H_{sh}$ ), and its suitability for cavity fabrication. Over time, the RF performance of bulk niobium cavities has consistently advanced, nearing the theoretical maximum performance limit ( $H_{sh} \sim 210$  mT) [1]. However, they are quite expensive and operate near their theoretical performance limits at temperatures below 2 K. Although further improvement has been achieved with nitrogen surface doping [2–5], long term solutions for SRF surface efficiency enhancement need yet to be pursued.

Nb<sub>3</sub>Sn and NbTiN are superconductors with A15 and B1 structures respectively, exhibiting a critical temperature  $T_c = 18.3$  K, normal-state resistivity ( $\rho_n$ ) between 8-20 nΩ·cm, and an upper critical field  $H_{c2} = 28$  T. Their critical temperatures are higher than that of Nb (9.3 K), which results in lower RF resistance at 4 K compared to Nb, leading to a different quality factor under these conditions. Utilising materials with a critical temperature greater than that of niobium enables the cavity to achieve performance parameters that are unattainable with conventional niobium cavities.

- Increasing a quality factor  $Q$  reduces heat produced and hence the electricity consumption of the cryogenic system during the RF cavity operation.
- Using high  $T_c$  superconducting materials allows to operate RF cavities at 4.2 K instead of 1.9 K used for the high-performance Nb cavities, more than doubling the efficiency of the cryogenic system.
- Increasing the cost-effective acceleration field  $E$  (at present the minimum cost is achieved at just over 30 MV/m) will result in massive saving in the infrastructure (tunnel, LHe supply and He recovery lines, electric cables, controllers, cryostats, pumps, etc). For example, 20% increase in the acceleration field allows 20% reduction of the acceleration line (compare: 4-km long tunnel for UK-XFEL instead of 5-km long or 50-km long tunnel for ILC instead of 60-km).

In recent years, there has been an extensive effort, with some degree of success, to convert a Nb cavity into Nb<sub>3</sub>Sn by alloying the inner surface of the cavity through Sn diffusion at high temperature near

1000 °C. In the past five years, there has been concerted effort to create such cavity using thin film deposition. This has several advantages to the existing diffusion method. Copper cavity, which has higher thermal conductivity, can be used instead of much more expensive Nb cavity.

In this study, superconducting Nb<sub>3</sub>Sn films are synthesised on different substrate such as sapphire, diamond turned copper and polished Nb, by DC magnetron sputtering from a single stoichiometric alloy Nb<sub>3</sub>Sn target. The flat sample deposition route is the most cost effective and ease of as compared to cavity coating as well ease of deposition. Hence, for deposition parameters optimisation the study is carried out with 2D geometry and then translated to 3D geometry.

The structural, morphological and superconducting properties of the films are investigated. The effect of deposition on different substrates is examined. The film properties are characterised by XRD, SEM, EDX, SIMS and XPS.

For SRF properties on 3D geometry, two types of cavities, 6 GHz open and closed copper cavity are used to measure  $Q_0$ , accelerating gradient  $E$  and critical temperature  $T_c$ . The choke cavity is also used to measure the same properties as well as RF surface resistance for flat samples.

## 2 Superconducting thin films on planar samples

### 2.1 Nb<sub>3</sub>Sn ON FLAT SAMPLES

#### 2.1.1 Optimisation of Nb<sub>3</sub>Sn deposition on Copper using Choke cavity (UKRI)

A series of Nb<sub>3</sub>Sn/Cu samples have been deposited by DCMS and HiPIMS, focussing on the effect of magnetron target power from 50 – 200 W at fixed deposition temperatures of ~ 615 °C. The film thickness was measured to be ~2.3 µm for each sample. Measurements of  $R_s$  vs sample temperature are shown in Fig. 1. For the samples deposited by DCMS, it can be seen that the RF performance improves as the target power is decreased down to 50 W. The sample deposited by HiPIMS with an average power 100 W was seen to have a higher  $R_s$  than the DCMS sample deposited at 100 W. Figure 2 shows a comparison of the  $R_s$  at 4.2 K vs target power, showing how the  $R_s$  improves by almost 2 orders of magnitude from ~ 20 to 0.4 µΩ with a decrease in target power from 200 to 50 W. Measurements of  $T_c$  by resonant frequency shift method, also demonstrate an improvement in  $T_c$  with decreasing target power for the samples deposited by DCMS, (the lowest power had  $T_c$  = 17.4 K and the highest power  $T_c$  = 16.4 K), with close agreement between RF and VSM measurements at both RAL (UKRI) and IEE (see section 5).

Figure 3 illustrates the surface resistance  $R_s$  vs sample temperature for different SC film studied in this program. As it can be seen Nb<sub>3</sub>Sn offers the lowest  $R_s$ . To optimizing the deposition temperature, we used  $T_c$  as a calibration parameter. The  $T_c$  measurement was done by four-point probe and it is shown in Fig. 4. It depicts that optimum temperature at least on sapphire is 570 °C.

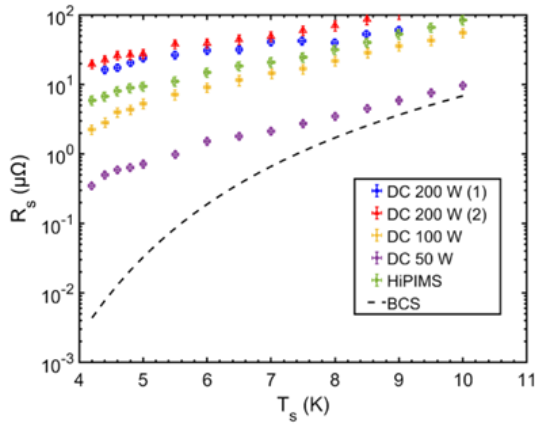


Figure 1. RF surface resistance at 7.8 GHz as a function of sample temperature for  $Nb_3Sn/Cu$  samples deposited by DCMS and HiPIMS at UKRI.

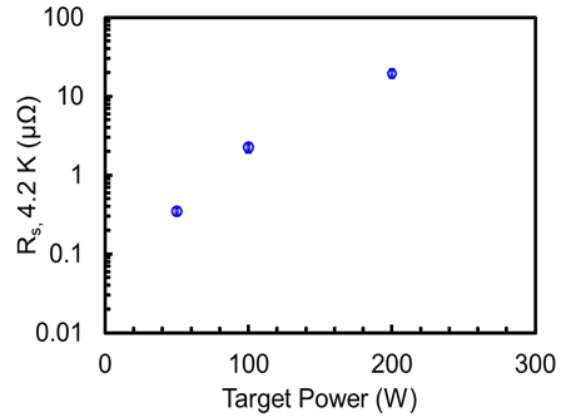


Figure 2. RF surface resistance at 4.2 K as a function of target power for  $Nb_3Sn/Cu$  samples deposited by L UKRIMS

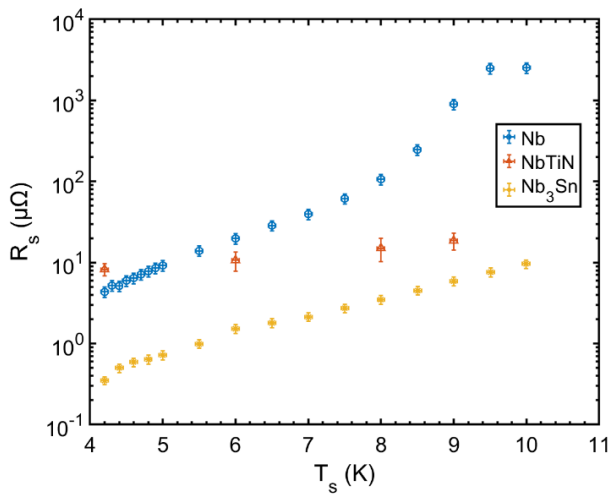


Figure 3: Surface resistance of different SC thin film on Cu

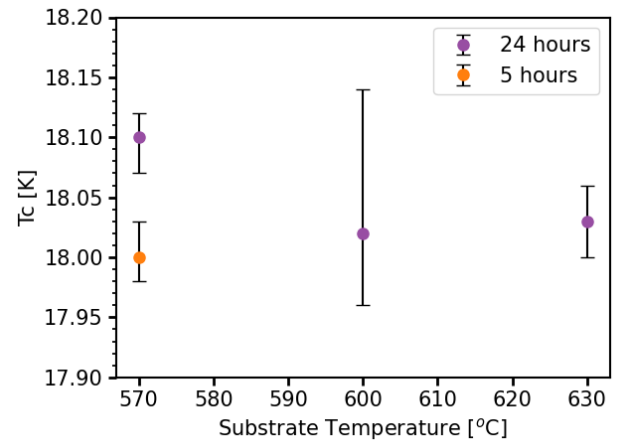


Figure 4: Optimisation of deposition temperature

In conclusion:

- Optimum deposition power for  $Nb_3Sn$  is established at 50 W DC power
- Optimum deposition of temperature for  $Nb_3Sn$  on Cu and Nb is at 570 and 650  $^{\circ}C$  for Cu and Nb substrate, respectively.
- For high  $T_c$ ,  $Nb_3Sn$  seems to be more suitable candidate for 4 K operation having lower  $R_s$  than NbTiN.

$Nb_3Sn$  was deposited on a 30  $\mu m$  thick Nb buffer layer, as illustrated in the section below, using a film deposition process conducted at INFN.

### 2.1.2 Optimisation of Nb<sub>3</sub>Sn on Cu, Nb and SAPPHIRE at INFN

At INFN, the study was focused on Nb<sub>3</sub>Sn, using a 4" planar magnetron and commercial targets [22, 23]. The goal is to identify the key process parameters that affect the  $T_c$  of Nb<sub>3</sub>Sn SC coatings and then to optimize them in order to obtain a recipe for growing coatings with  $T_c$  close to the nominal value that can be scaled to elliptical copper cavities.

The production of Nb<sub>3</sub>Sn films at INFN-LNL follows a standard procedure with a high level of control and reproducibility. The films are 1  $\mu\text{m}$  thick and deposited in Ar atmosphere using a commercial, stoichiometric target, on different substrates: Al<sub>2</sub>O<sub>3</sub>, Cu, Cu pre-coated with a Nb buffer layer of varying thickness, and bulk Nb. After deposition, the films are characterized by measuring the  $T_c$ , inspecting their surface and cross-section via SEM, analyzing their elemental composition via EDS and crystalline properties via XRD, and finally, measuring their RF surface resistance via the production of a QPR sample. The deposition parameters are tuned based on the characterization results in a tight-feedback process. The optimal sputtering pressure, surface current density applied to the target, deposition temperature, and annealing temperature and duration are determined based on the optimization of the film  $T_c$  (Fig. 5 (a) and (b)). The Nb buffer layer is implemented to prevent copper-tin interdiffusion and plays a key role in the film quality, also demonstrated first by the dependence of the  $T_c$  on the thickness of the buffer layer (Fig. 5 (c)). The accommodation effect provided to the Nb<sub>3</sub>Sn film by the increasing thickness of the buffer layer is demonstrated by the trend of the lattice parameter of the film and of the buffer layer itself (Fig. 5 (d)). With the  $T_c$ -driven tuning of the deposition parameters and the study of the buffer layer thickness effect, the following optimized coating was obtained:

- Low cathode surface current density  $< 2 \text{ mA/cm}^2$ ;
- Deposition pressure  $\sim 2 \times 10^{-2} \text{ mbar}$ ;
- No annealing;
- Deposition temperature range 600 – 650  $^{\circ}\text{C}$ ;
- Nb buffer layer thickness  $\geq 30 \text{ }\mu\text{m}$ .

This recipe delivered films on Cu and Nb buffer layer substrate of 30  $\mu\text{m}$  with a  $T_c \geq 17 \text{ K}$  and an RF surface resistance of 23  $\text{n}\Omega$  at 4.5 K, 20 mT and 400 MHz. Further characterization of the films deposited according to the optimized recipe demonstrated a homogeneous morphology (Fig. 5 (e) and (f)); a not yet optimal performance in terms of magnetic flux trapping due to thermoelectric currents induced by cooldown dynamics (Fig. 1 (g)); a good values of substrate thermal conductivity, which is not affected by the presence of the thick Nb buffer layer (Fig. 5 (h)); a good value of the superconducting gap, consistent with literature for a film with the given  $T_c$  and composition (Fig. 5 (i)); a slight improvement in terms of crystallinity following post-coating treatments such as Flash Lamp Annealing FLA at HZDR (Fig. 5 (l)).



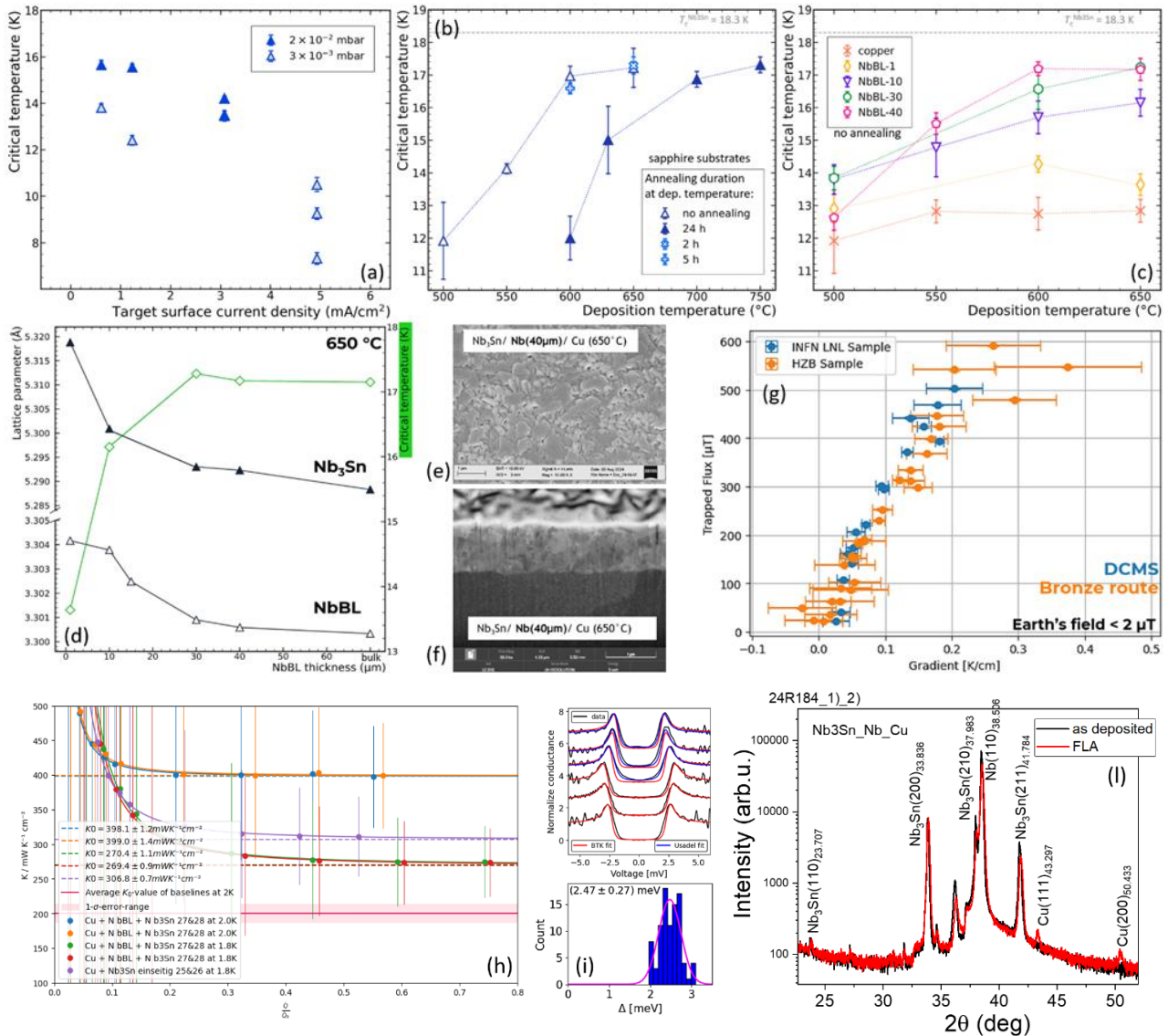


Figure 5. INFN results: (a)  $T_c$  against target surface current density for films deposited on Al<sub>2</sub>O<sub>3</sub> at two different Ar pressures. (b)  $T_c$  against deposition temperature for films annealed for 24 hours, not annealed, and annealed at intermediate durations, deposited on Al<sub>2</sub>O<sub>3</sub> at 0.02 mbar. (c)  $T_c$  against deposition temperature for films deposited on Cu and Cu plus Nb buffer layer of increasing thickness, at 0.02 mbar Ar pressure and not annealed. (d) Lattice parameter of Nb<sub>3</sub>Sn films deposited on Nb buffer layer and lattice parameter of the Nb buffer layer itself as a function of the buffer layer thickness. The corresponding  $T_c$  of the samples is also indicated. (e) SEM micrograph of the surface of a Nb<sub>3</sub>Sn film deposited according to the optimized recipe. (f) SEM micrograph of the cross section of a Nb<sub>3</sub>Sn film deposited according to the optimized recipe. (g) Trapped flux versus thermal gradient across Nb<sub>3</sub>Sn sample deposited according to the optimized recipe via DCMS. The data are compared to what obtained for a sample produced at HZB via bronze route. (h) Thermal transmittance of Nb<sub>3</sub>Sn samples deposited according to the optimized recipe on Nb buffer layer (30 μm) and directly on Cu, compared to bulk Nb baseline. (i) Superconducting energy gap of a Nb<sub>3</sub>Sn sample deposited according to the optimized recipe. (l) XRD diffractogram of a Nb<sub>3</sub>Sn sample deposited according to the optimized recipe before and after post-deposition FLA treatment.



### 2.1.3 Nb<sub>3</sub>Sn deposition on Silicon at USI

Parameter optimization of Nb<sub>3</sub>Sn deposition via RFMS from stoichiometric target has been started to explore the possibility of Nb<sub>3</sub>Sn film's application as a top layer in the S-I-S multilayer structure for SRF cavities. Pieces of Si<100> and sapphire wafers were used as a substrate. First test depositions demonstrated, on the one hand, the presence of the target Nb<sub>3</sub>Sn cubic phase but the absence of a pronounced grain structure and superconducting properties, and, on the other hand, the presence of a clearly defined structure with large grains but a poorly crystalline phase (large contribution of an amorphous phase), as well as the presence of an additional unidentified phase. Optimization of deposition parameters continues; measurements of the critical temperature  $T_c$  are ongoing. The planar SEM micrograph is presented in Fig. 6.

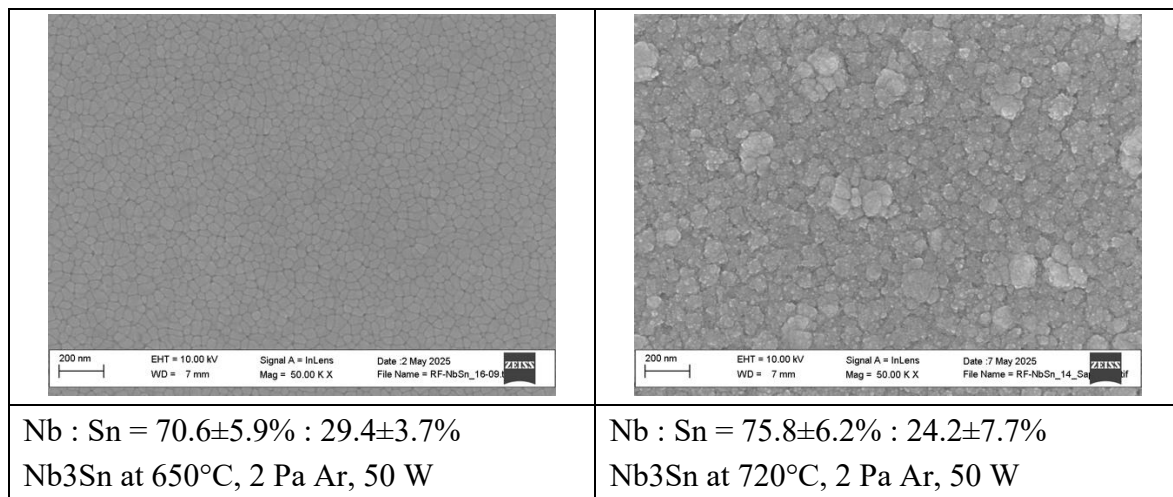


Figure 6: SEM of Nb<sub>3</sub>Sn deposited on Si (a) and sapphire (b)

## 2.2 NbTiN DEPOSITION

### 2.2.1 Deposition of NbTiN on flat sample at USI by DCMS

NbTiN was suggested as a candidate material for a top film coating in a S-I-S multilayer structures. In the previous studies, the optimized deposition processes for HiPIMS-Nb superconducting layer and DCMS AlN insulating layer were established. The current research was focused on the optimization of the deposition parameters of NbTiN superconducting thin film in the coating system at the University of Siegen. At the very beginning, a co-sputtering process from independent Ti and Nb targets was considered. The deposition system and target arrangement is shown in Fig. 7. However, the results of the co-NbTiN study were unsatisfactory due to low  $T_c$  of the deposited films (<15 K) and non-uniformed covering of the substrate because of the geometrical features (non-confocal cathode arrangement) of the coating system. In this case, deposition study and parameter optimization of NbTiN via DCMS from an alloy target NbTi (80/20 wt%) were carried out by utilization of a commercial coating system from CemeCon CC800/9. Pieces of Si<100> and polished Cu were used as a substrate. The influence of such parameters as the total deposition pressure, cathode power, substrate bias and nitrogen content in the gas mixture on the critical temperature of the

resulting DC-NbTiN films was studied. The deposition temperature was fixed to the value of around 250 °C due to limitations in the heating capabilities of the coating system.

- a) Deposition pressure: decreasing of the total pressure during the deposition led to the film densification as shown in figure 10 and 11, smoothening the film surface and increase of the  $T_c$ . The highest  $T_c = 14.4(1)$  K was reached at a deposition pressure of 0.5 Pa (9%  $N_2$ , 400 W) as shown in figure 9.
- b) Cathode power: increase of the cathode power led to the film densification and increase of the critical temperature. The highest  $T_c = 14.7(1)$  K was reached at a cathode power of 600 W (9%  $N_2$ , 0.9 Pa).
- c) Nitrogen content: variation of a  $N_2$  content in a gas mixture ( $N_2/Ar$ ) demonstrated that there is an optimal  $N_2$  range (5%-9%) during the deposition where films show high  $T_c$  values. Increasing of  $N_2$  in the gas mixture leads to the narrowing of the film grains, reducing the film crystallinity and decreasing of the  $T_c$ . The highest  $T_c = 14.4(1)$  K was reached at a  $N_2$  content of 5% (400 W, 0.9 Pa). Interestingly, the relationship between an optimal  $N_2$  range and  $T_c$  depends on the cathode power as well: at increased cathode powers the optimal  $N_2$  range shifts to a higher  $N_2$  content probable because more  $N_2$  is required to form a NbTiN phase at increased deposition rates.



*Figure 7. Industrial coating system CC800/9 (CemeCon).*

In addition, the results of DC-NbTiN deposition study and influence of the deposition parameters were confirmed by Positron Annihilation Lifetime Spectroscopy (PALS) experiments at HZDR (Dresden, German). The first results demonstrate significant reduction in the number of voids/nanopores in the film structure by densification due to deposition at low pressures (below 0.7

Pa) and high cathode powers (increasing from 250 to 600 W) as shown in Fig. 8. As the next step in DC-NbTiN optimization, deposition experiments will be conducted at higher substrate temperatures, which has become possible due to the recent heater modifications of the deposition system.

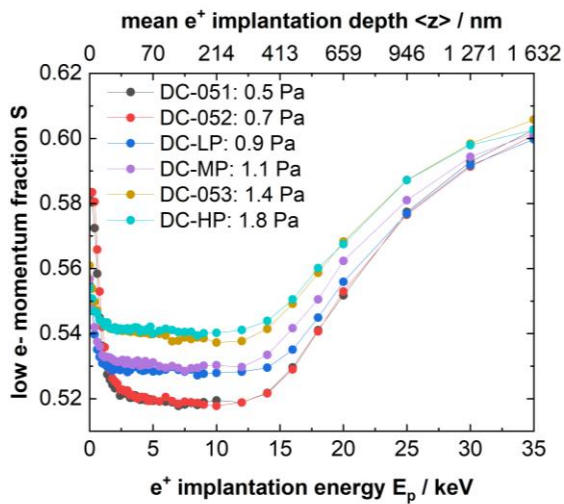


Figure 8. PALS experiments on DCMS-NbTiN, Effect of deposition pressure variation.

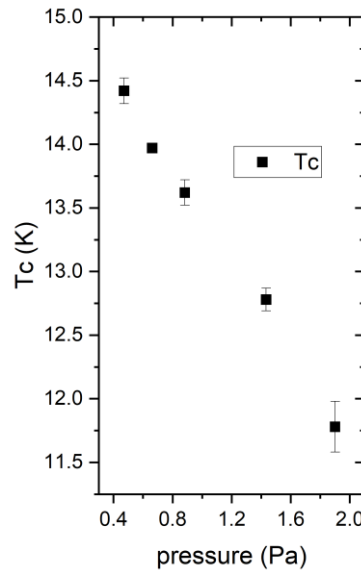


Figure 9. DCMS-NbTiN,  $T_c$  vs deposition pressure.

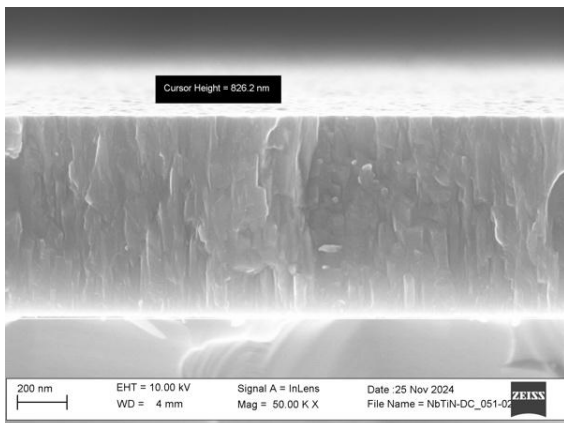


Figure 10. DCMS-NbTiN 400 W, 9% N<sub>2</sub>, Bias = -50 V, 0.5 Pa.

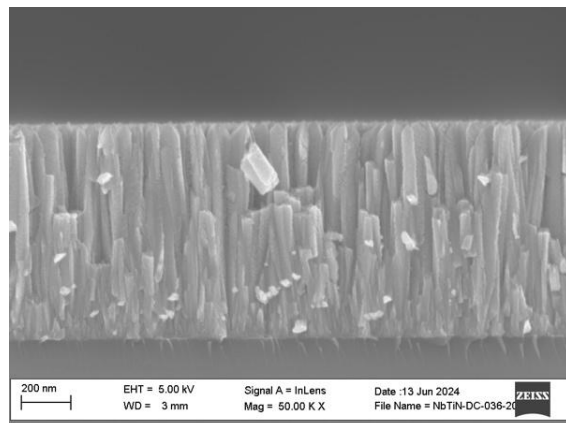


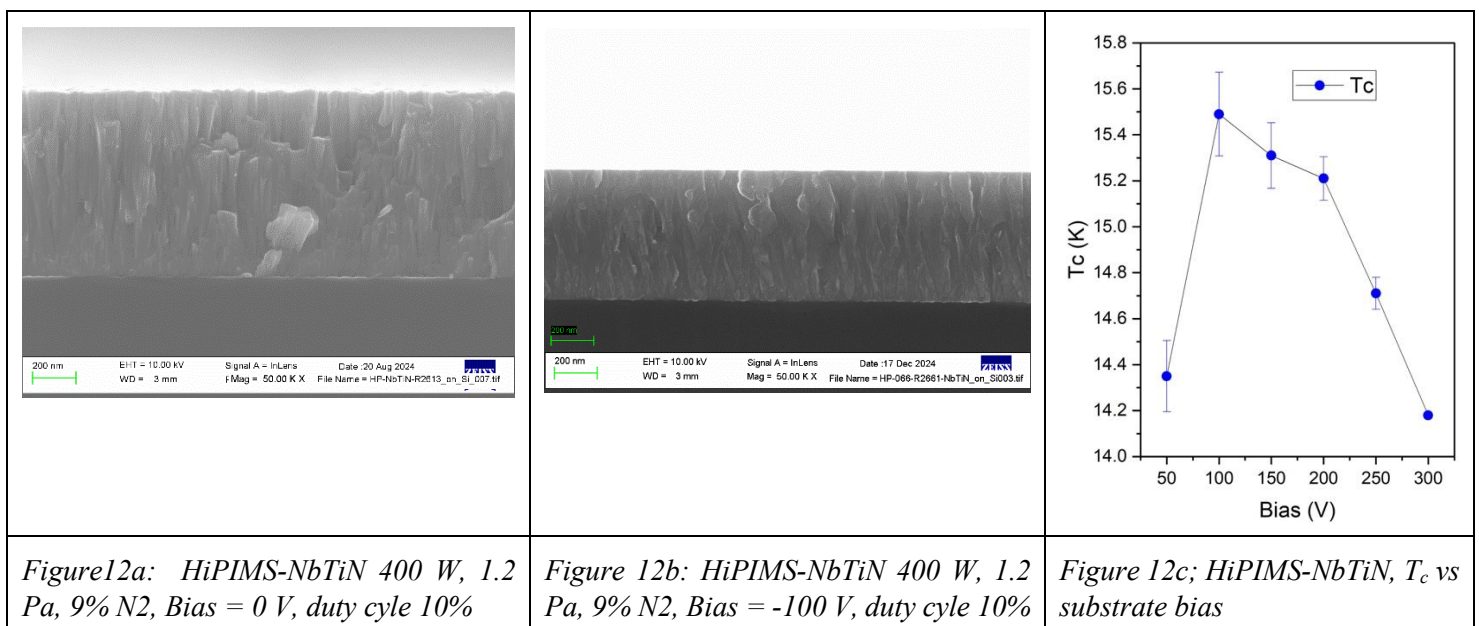
Figure 11. DCMS-NbTiN 400 W, 9% N<sub>2</sub>, Bias = -50 V, 1.8 Pa.

## 2.2.2 NbTiN deposition by HiPIMS (study was carried out by Bharath Reddy Lakki Reddy Venkata)

Magnetron sputtering via HiPIMS method allows to deposit thin films with denser film structure, smother surface and better film performance in comparison with a classical DCMS. In this case, deposition study and parameter optimization of NbTiN via HiPIMS from an alloy target NbTi (80/20 wt%) were carried out by utilization of a commercial coating system from CemeCon CC800/9. The following deposition parameters were selected as the main ones in the optimization process: deposition pressure, parameters of the HiPIMS cathode (pulse width and pulse frequency), substrate bias. Variation of a N<sub>2</sub> content in a gas mixture (N<sub>2</sub>/Ar) demonstrated the same tendency as it was demonstrated during the deposition study of DC-NbTiN where the optimal N<sub>2</sub> range lies in the range between 5 and 9% of nitrogen. The highest  $T_c = 15.1(1)$  K was reached at N<sub>2</sub> content of 5% (400 W, 1.6 Pa, -50 V bias, 20% duty cycle,  $T_{\text{substrate}} = 180$  °C).

- Deposition pressure: despite the similarity of the two methods, variation of the deposition pressure in HiPIMS method shows the existence of a specific pressure region where the critical temperatures take higher values. The highest  $T_c$  of 14.3(1) K was reached at a deposition pressure of 1.6 Pa (400 W, 9% N<sub>2</sub>, -50 V bias, 10% duty cycle,  $T_{\text{substrate}} = 180$  °C). By low deposition pressures, residual stress is created what could negatively affect the superconducting performance of NbTiN films.
- Substrate bias: application of a negative substrate bias leads to the improvement of the film microstructure, film densification and smothering the film surface. However, application of too high bias causes an accumulation of the internal stresses in the film and reduction of  $T_c$ . The highest  $T_c = 15.5(2)$  K was reached at a substrate bias of -100 V (400 W, 9% N<sub>2</sub>, 1.6 Pa, 10% duty cycle,  $T_{\text{substrate}} = 300$  °C) as shown in Fig. 12 (a-c).

As the next step in HiPIMS-NbTiN optimization, deposition experiments will be conducted at higher substrate temperatures, which has become possible due to the recent heater modifications of the deposition system.





## 2.3 V<sub>3</sub>SI DEPOSITION ON FLAT SAMPLE

Deposition parameters of Vanadium Silicide (V<sub>3</sub>Si) thin films have been explored to assess V<sub>3</sub>Si suitability as a potential alternative to Nb for SRF cavity applications. Initial films were deposited on sapphire wafer using pulsed DC magnetron sputtering of a 50.5 mm V:Si alloy target with fixed deposition parameters:

Average power: 300 W	Pulse width: 1.1 $\mu$ s
Frequency: 350 kHz	Pressure: $5 \times 10^{-3}$ mbar

Substrate temperature was increased for each subsequent deposition leading to a sharp increase in  $T_c$  to a maximum of  $14.7 \pm 0.1$  K, a few K lower than reported bulk samples with inconsistency in  $T_c$  between films deposited at high temperatures. HiPIMS was employed to improve consistency and density of the film structure. Films were also deposited on Nb substrates using deposition parameters:

Average power: 300 W	Pulse width: 10 $\mu$ s
Frequency: 100 Hz	Pressure: $5 \times 10^{-3}$ mbar

Superconducting properties were assessed via four-point probe (sapphire) and SQUID-VSM (Nb), with the highest  $T_c$  measured at 14.85 K (sapphire) and 13 K (Nb). Grazing incidence XRD confirmed the formation of the desired A15 cubic phase of V<sub>3</sub>Si, with no secondary V-Si phases observed. Peak broadening across diffraction spectra indicates randomly oriented small crystallites. XPS measurements confirmed the presence of metallic vanadium and V-Si bonding states; however, carbon contamination (C-C and carbide) and surface oxygen were also detected. Contaminants are presumed to originate from atmospheric exposure and residual gases during deposition. Initial SEM analysis revealed the formation of crystallites in V<sub>3</sub>Si films on sapphire, with noticeable voids between grains indicative of preferential nucleation as shown in Fig. 13.

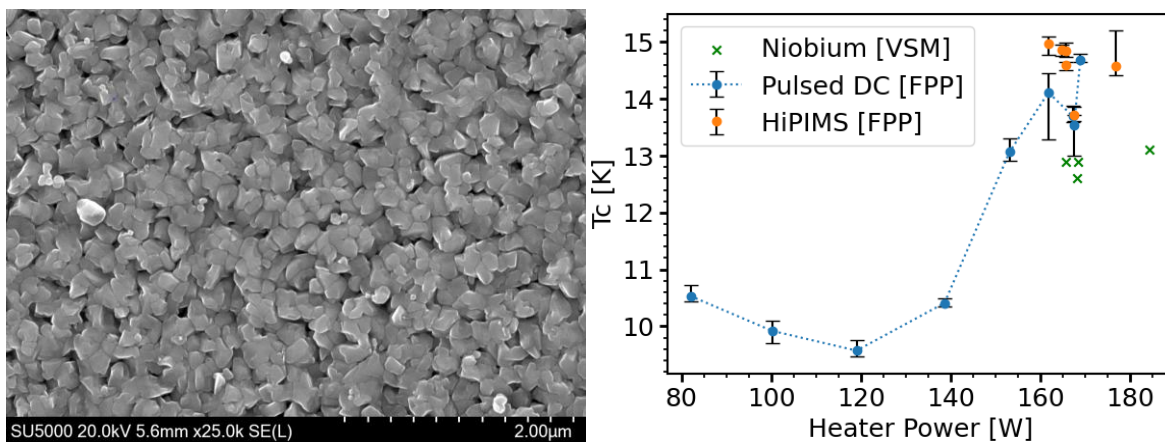


Figure 13: (a) Planar SEM monograph of V<sub>3</sub>Si deposited on Sapphire, (b) dependence of  $T_c$  on deposition temperature.

Optimization of deposition parameters is ongoing. Future work will explore adjustments to HiPIMS duty cycle, introduction of bipolar pulsing, and post-deposition annealing (UHV, flash, or laser-based) to improve crystallinity and reduce defects. The results demonstrate promising but non-optimal superconducting behavior, with further improvements required to approach bulk performance values and enable practical application in SRF cavities.

## 2.4 CHARACTERISATION OF FLAT SAMPLES VIA MAGNETIZATION MEASUREMENTS

Magnetic flux penetration into the superconducting thin films in DC conditions was investigated by means of magnetization measurements. Using a commercial Vibrating Sample Magnetometer (VSM) set-up, virgin DC magnetization curves and magnetization loops were measured on small planar thin film samples of approximately  $2\text{ mm} \times 2\text{ mm}$ , prepared with the help of a laboratory cut-off machine. The main characteristic determined from the magnetization curves was the first flux entry field  $H_{en}$ , determined as the applied field at which the magnetic flux starts entering the superconductor's volume.

Dependence of the magnetic moment on temperature, measured in a constant small magnetic field, was utilized to determine the critical temperature  $T_c$  of the superconducting film.

The efforts were targeted on development of resonant cavity coating with a material other than Niobium. The main emphasis has been put on testing the NbTiN and Nb<sub>3</sub>Sn materials.

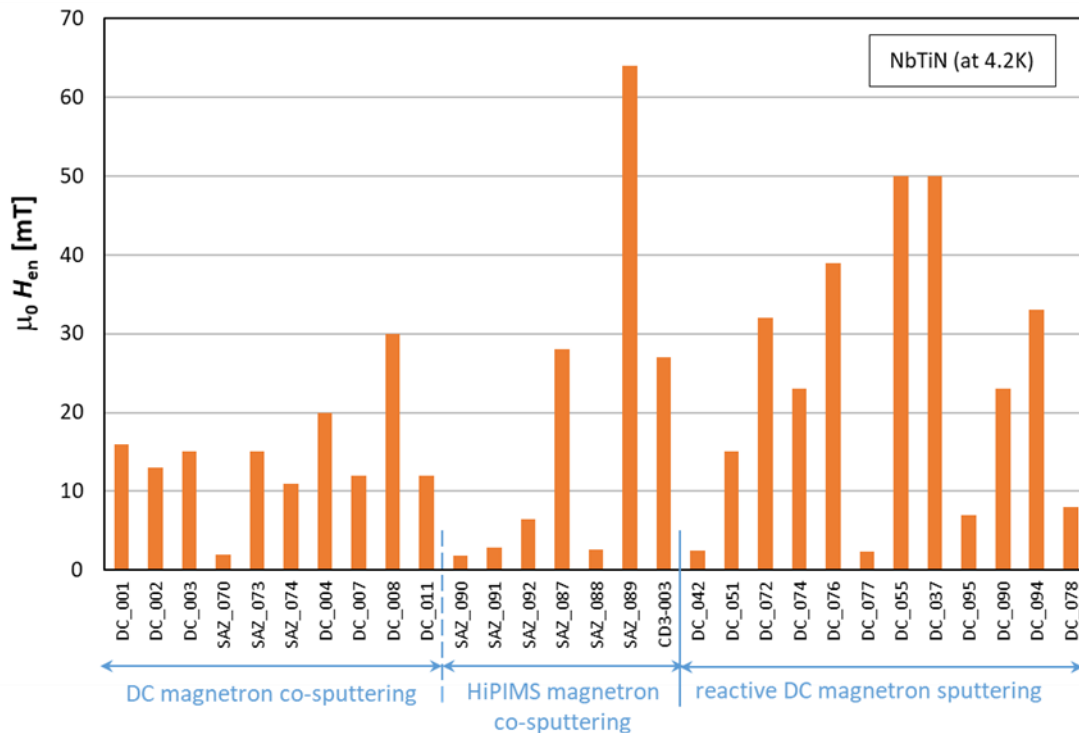


Figure 14. First flux entry fields  $H_{en}$  of the investigated NbTiN thin films.

The investigated NbTiN films were deposited on Si substrates, employing the DC and HiPIMS magnetron co-sputtering methods and the reactive DC magnetron sputtering via NbTi alloy targets. The first flux entry field and the critical temperature values determined for the individual samples are summarized in Figs. 14 and 15, respectively.

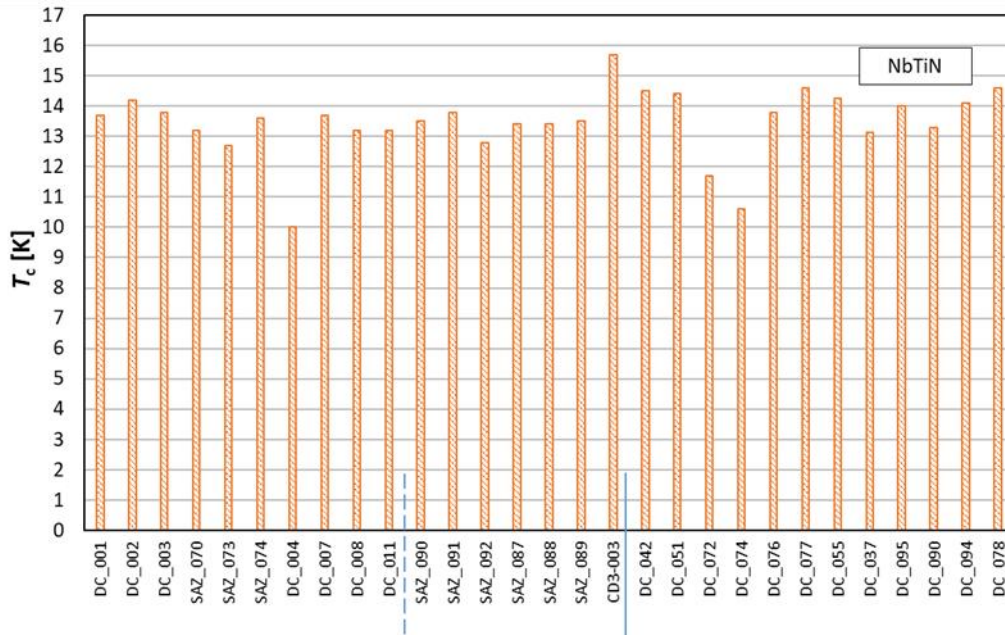


Figure 15. Critical temperatures ( $T_c$ ) of the investigated NbTiN thin films.

On average, the highest  $H_{en}$  values are seen in the set of samples prepared via the reactive DC magnetron sputtering (using NbTi alloy targets). Regarding the critical temperatures, no particular differences are observed among the sputtering methods, the typical values ranging approximately from 13.0 to 14.5 K.

The Nb<sub>3</sub>Sn thin films were deposited on Cu and sapphire substrates. Three of the Cu substrate samples also contained an additional Nb buffer layer between the Cu substrate and Nb<sub>3</sub>Sn layer, 9, 40 and 50  $\mu\text{m}$  thick. The  $H_{en}$  and  $T_c$  values of the Nb<sub>3</sub>Sn samples are summarized in Figs. 16 and 17. The results show that introducing the rather thick Nb buffer layer notably helps to increase the first flux entry field  $H_{en}$ . The  $T_c$  values are quite similar among all the samples, excluding just three outliers they all fall between 16.0 and 17.5 K.



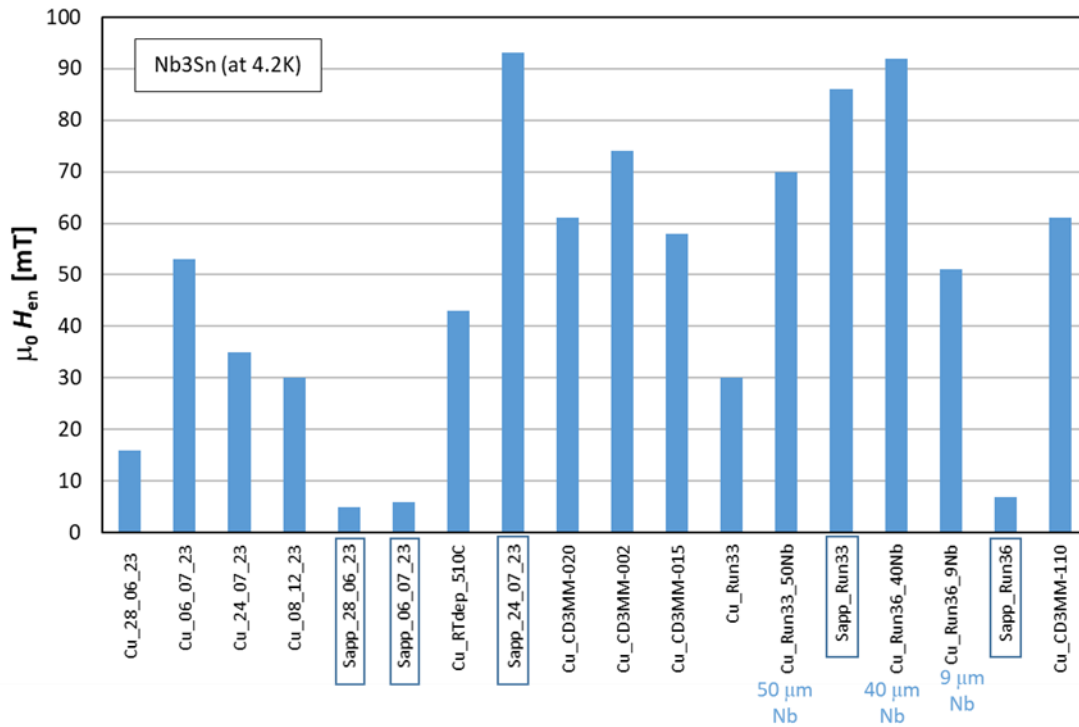


Figure 16. First flux entry fields  $H_{en}$  of the investigated  $Nb_3Sn$  thin films. Samples with the Nb base-layer and the sapphire substrate samples (rectangular framing) are indicated.

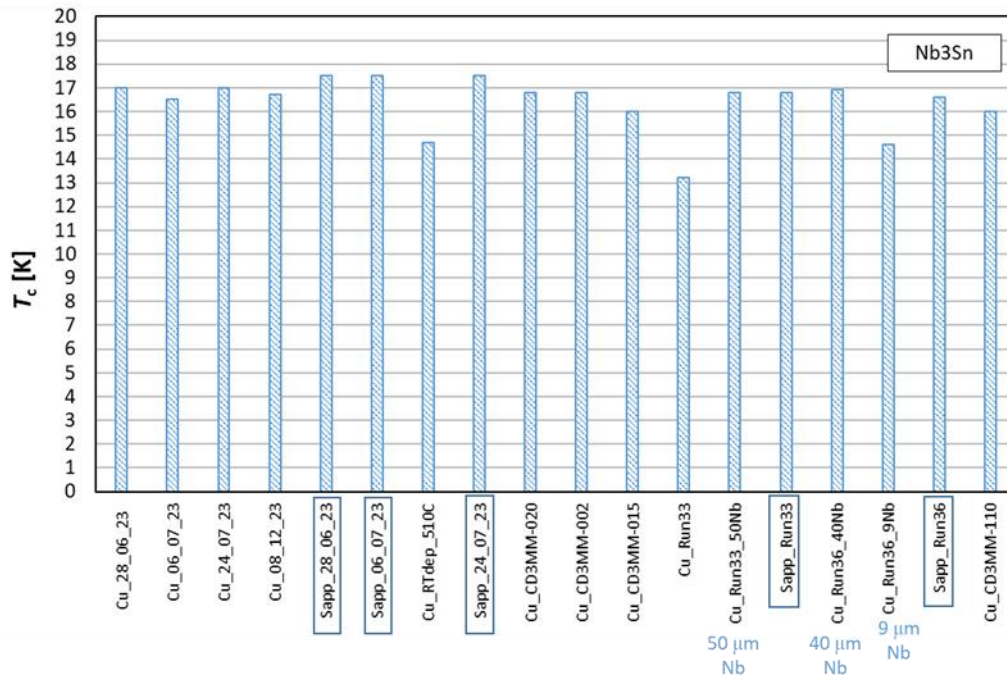


Figure 17. Critical temperatures ( $T_c$ ) of the investigated  $Nb_3Sn$  thin films. Samples with the Nb base-layer and the sapphire substrate samples (rectangular framing) are indicated.

## 3 Deposition on 6 GHz Copper cavity

### 3.1 NbTiN deposition of 6 GHz closed copper cavity

6 GHz cavity prepared by PEP at INFN, deposited by reactive sputtering at UKRI with NbTiN using pulsed DC, and mixed target in partial pressure of nitrogen and krypton gas. The chosen target was solely depicted due to lack of alternative target in cylindrical form. Hence, as a compromise, for high  $T_c$  superconducting alloy the NbTi N was chosen. Prior to deposition on cavity, film was deposited on 2-inch diameter copper and sapphire disk.

#### 3.1.1 Deposition chamber at UKRI

Figure 18 (a-e) depict the deposition facility and the internal assembly. A large electromagnet provides the magnetic field, this type of magnetron will provide a uniform plasma over the entire target hence results in a better film uniformity. Six 240 W halogen lamps, filled with Kr gas provides heating for disposition. A 0.5 mm thick stainless-steel sheet provides heat shield allowing temperature as high as 800 °C to be reached. Prior to cavity deposition, for each set of target combination film were deposited on both copper and sapphire disk for calibration. The films were then analysed for critical temperature using four point probe and dc magnetic field, film morphology in both planar and cross-section, film composition using XRD, EDS. This allowed optimisation of deposition parameters.

#### 3.1.2 Deposition chamber at INFN

The dimensional constrain of the 6 GHz cavities imposed the design of a compact sputtering source, where cathode, 6 GHz cavity and IR lamp, are mounted together (with the appropriate electrical insulation) on a CF100 flange.

In contrast with the LHC different configurations where the magnetic field is generated with magnets inside the target, in INFN for the coating of the 6 GHz cavities a post magnetron cylindrical configuration is adopted, in which the source of the magnetic field is placed outside the vacuum chamber. In the Fig. 19, the coating system scheme for the 6 GHz cavities is visible. The cavity inside the vacuum chamber, is placed approximately at the center of the coil, where the magnetic field lines are homogeneous and parallel to the cathode surface.

The coating system has long been used to produce thick-film cavities in Nb, showing excellent results in terms of both Q and accelerating field (REF). The temperature limit for this system is between 650 and 700 °C, above which the copper cavity begins to soften too excessively.

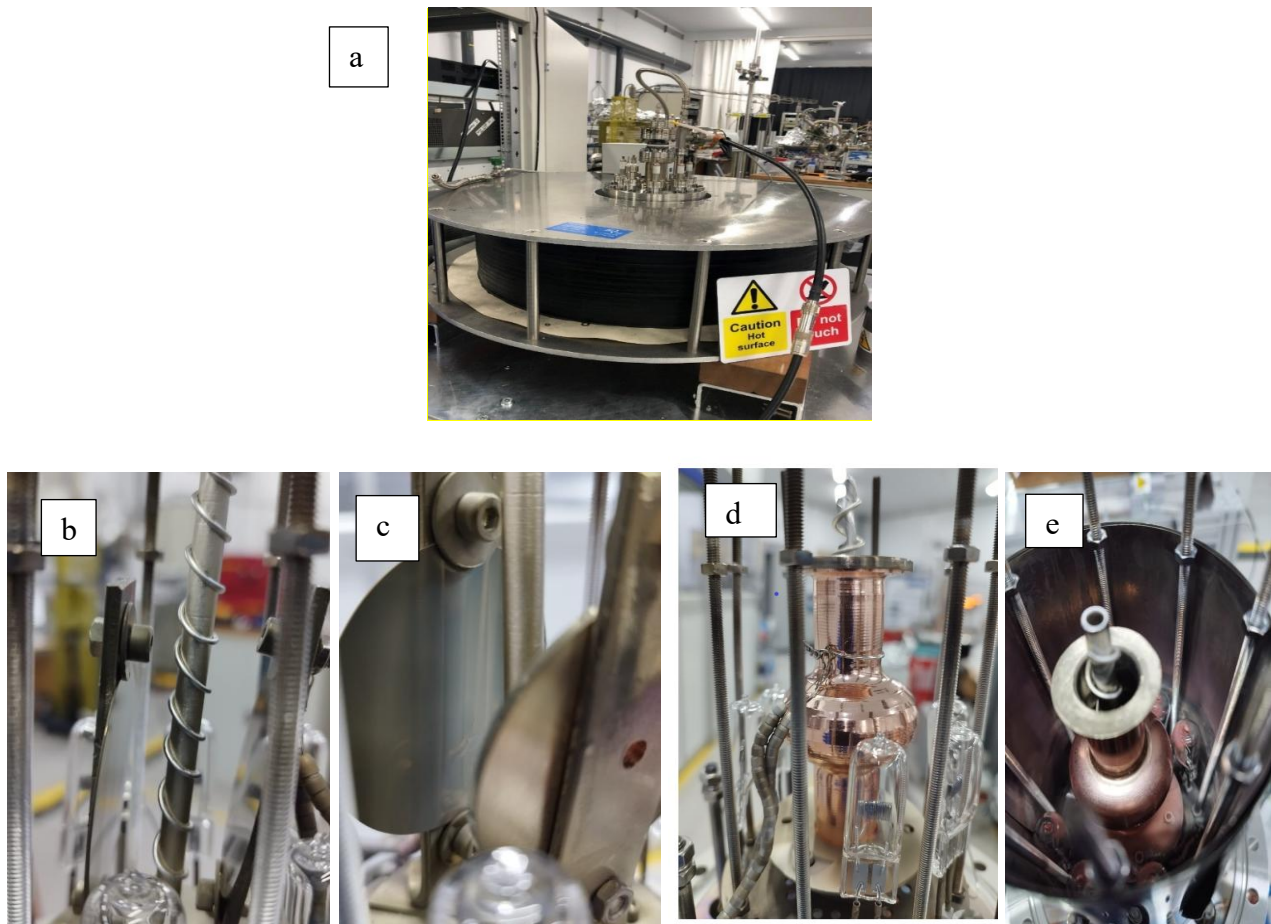


Figure 18: (a) Deposition chamber, (b) Target, (c) Flat substrates, (d) Cavity with heating bulb assembly, (e) Stainless steel heat shield.

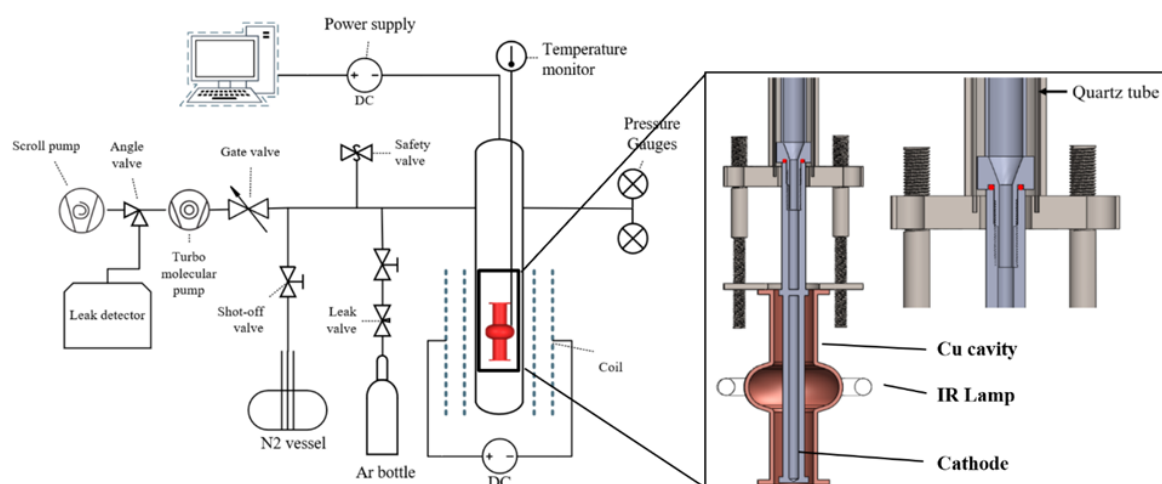


Figure 19. The deposition facility at INFN. Post-magnetron configuration for 6 GHz cavities coating.

### 3.1.3 SRF measurement facility at INFN

The RF characterizations for the 6 GHz cavities take place in the Surface Technologies and Superconductivity Service at LNL. The instrumentation includes a dedicated cryostat for the RF test of the 6 GHz cavities (with the possibility to measure 3 cavities simultaneously), a 500-liter dewar for the liquid helium, an exclusive liquid nitrogen tank, and an electronic set up for the measurement. The system possesses the capability to register the  $Q$  vs  $E_{acc}$  curve, the monitoring of the temperature, cryostat pressure, radiation, helium level, and cavity pressure.

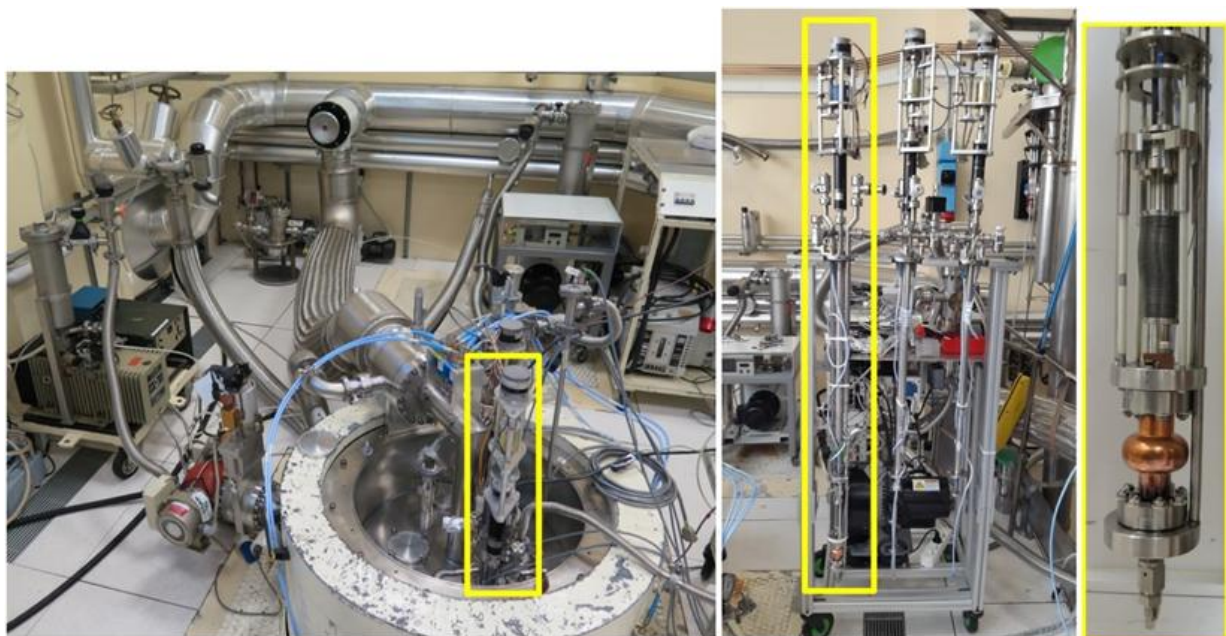
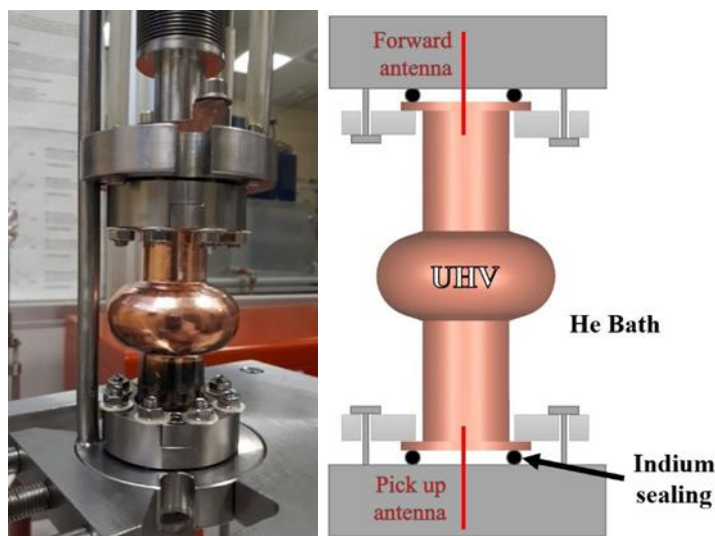


Figure 20. (a) Cavity mounted in RF stand..(b) Pictorial representation with antennas. (c) RF stand (yellow) inside cryostat (left), outside (center), and zoomed (right).



At LNL a Class 100 cleanroom is available for the manipulation of the SRF cavities for the preparation for the RF test. The cavity is inspected and mounted in the RF stand, in which the cavity will be pumped, and the inner surface will be in vacuum. In addition, two antennas are installed: a movable coupler and one pick up antenna on the other side of the cavity. The cavity is mounted in a stainless-steel (SS) structure that will be afterward pumped to pressure approximately  $1 \times 10^{-8}$  mbar prior the RF test. The 6 GHz cavity mounted in the stand and the pictorial representation of the antennas are shown in Fig. 20, where is represented the indium vacuum and cryogenic sealing between the cavity and the SS structure.

The system includes also a fluxgate magnetometer (for flux-expulsion measurements) and 2 thermometers CERNOX, located in the equator of the cavity.

### 3.1.4 Deposition parameters and analysis at UKRI

The optimised deposition parameters was as follows:

Pulsed DC Magnetron Sputtering

- 200 W Power
- 350 kHz Repetition rate
- 1.1  $\mu$ s Duty Cycle
- 600 °C Substrate temperature
- Ratio of Kr or He to N<sub>2</sub> (2:1).

Three sets of target combination were used.

- Target 1: Nb Tube with Ti wire
- Target 2: Nb<sub>37</sub>Ti<sub>63</sub> with Nb Wire
  - Ratio of Nb to Ti can be varied but, target to substrate distance is important for uniform stoichiometry
- Target 3: Nb<sub>37</sub>Ti<sub>63</sub> single stoichiometry

The results are summarized below.

*Table 1. Critical temperature as determine by four point probe and DC magnetisation on sapphire and copper substrate respectively.*

Target	Process Gas	$T_c$ [K] by resistive on sapphire substrate	$T_c$ [K] by DC magnetic on copper substrate
Nb rod with Ti wire	Kr + N <sub>2</sub>	<b>17.41</b> <sup>+0.08/-0.05</sup>	
NbTi rod with Nb wire	Kr + N <sub>2</sub>	<b>17.68</b> <sup>+0.06/-0.05</sup>	<b>16.5</b>
NbTi rod with Nb wire	He + N <sub>2</sub>	<b>17.57</b> <sup>+0.02/-0.01</sup>	<b>delamination</b>
NbTi rod	Kr + N <sub>2</sub>	<b>14.95</b> <sup>+0.09/-0.04</sup>	<b>14.1</b>

**Cavity 1:** Cu 6 GHz cavity coated with a thin Nb film, see Fig. 21.

Internally, after HPR process, a coating delamination appeared.

$$Q(4.2\text{ K}) = 2.4 \times 10^6 @ E_{\text{acc}} = 0.2\text{ MV/m}, Q = 1 \times 10^6 @ E_{\text{acc}} = 1.2\text{ MV/m}$$

$$Q(1.8\text{ K}) = 4.4 \times 10^6 @ E_{\text{acc}} = 0.2\text{ MV/m}$$

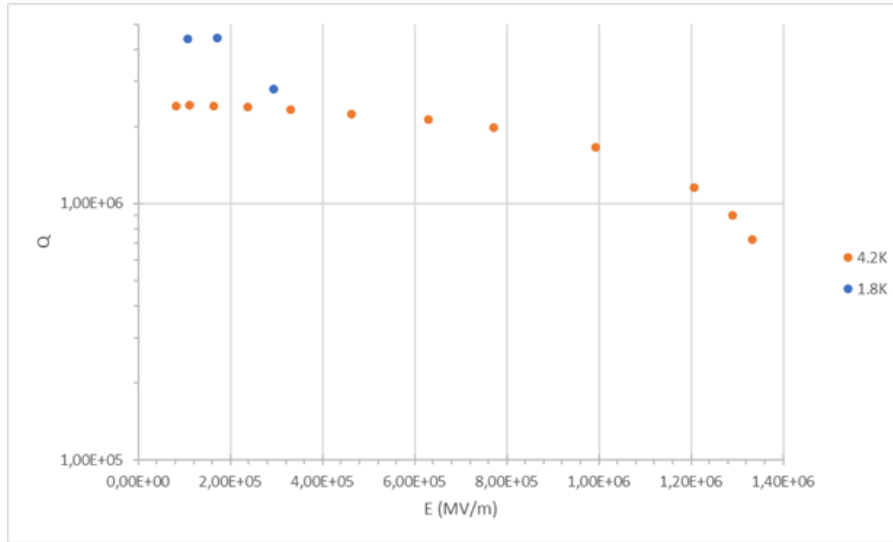


Figure 21. *Q* factor vs accelerating gradient at  $T = 4$  and  $1.8\text{ K}$ .

**Cavity 2 (Cav75):** Cu 6 GHz cavity coated with a thin NbTiN film, see Fig. 22.

By flux expulsion a  $T_c = 16.8\text{ K}$  has been measured.

$$Q(4.2\text{ K}) = 4.3 \times 10^6 @ E_{\text{acc}} = 0.18\text{ MV/m (cavity quench @ } E_{\text{acc}} \sim 0.28\text{ MV/m)}$$

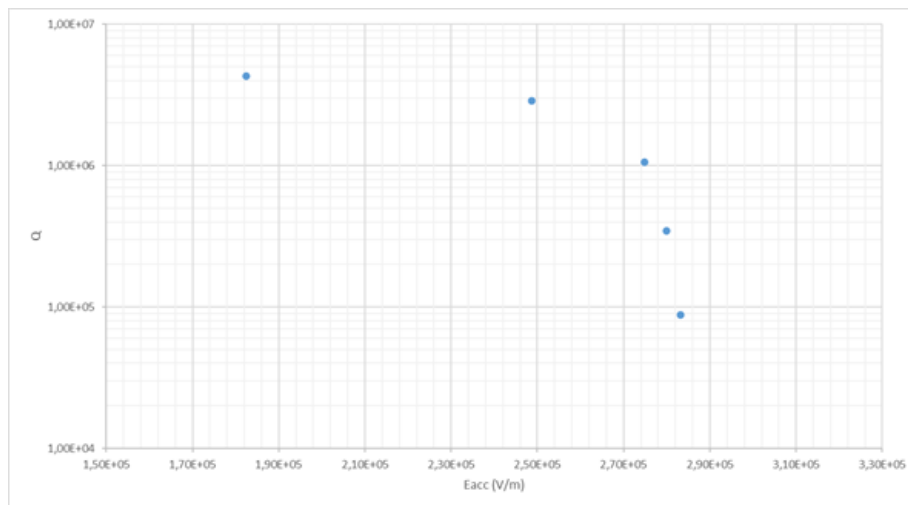
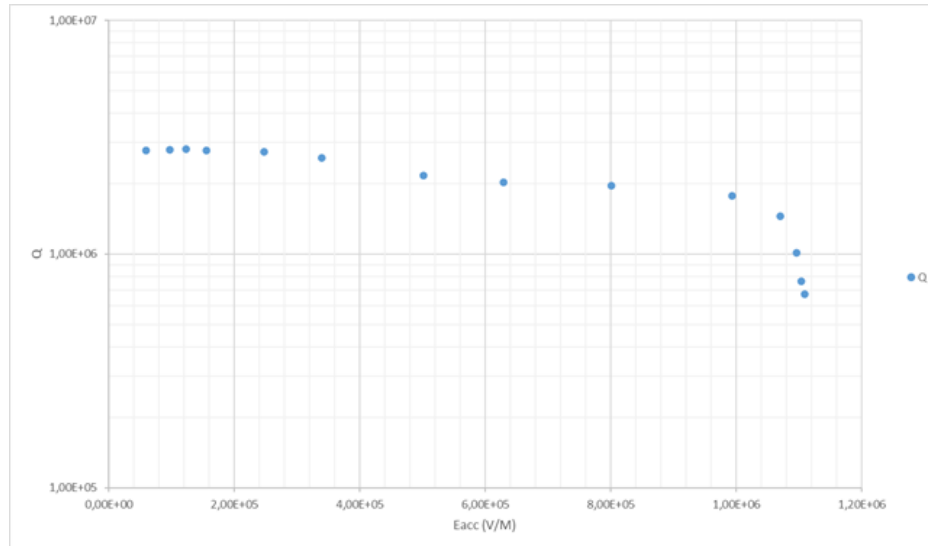


Figure 22. *Q* factor vs accelerating gradient at  $T = 4\text{ K}$ .

**Cavity 3 (Cav62):** Cu 6 GHz cavity coated with a thin NbTiN film, see Fig. 23.

Measured  $T_c \approx 16.2$  K.

$Q(4.2 \text{ K}) = 2.8 \times 10^6$  @  $E_{acc} = 0.2 \text{ MV/m}$  (cavity quench @  $E_{acc} \sim 1.1 \text{ MV/m}$ )





Tables 1 and 2 show, different target combination resulted in different film composition. However, beside the single stoichiometric target (Nb<sub>3</sub>7Ti<sub>6</sub>3), all other combination had superconducting critical temperature  $T_c = 17.5$  K, on sapphire that is very close to value of 18 K reported in various literature. The film deposited on copper matched values determined from the cavity.

The RF measurement of film deposited on 6 GHz cavity showed a low-quality factor  $Q = 10^6$  which is a factor 10 lower than what was expected, this combined with low accelerating gradient of 1.1 MV/m necessitate for more study for B1 superconducting material.

In this study, we used 6 GHz cavity, to open the path to optimise the deposition parameters for high superconducting material with  $T_c$  higher than of Nb, such as B1 and A15, that can then be extrapolated to 1.3 GHz cavity deposition. This was based on the successful study of Nb coating at INFN. However, due to confined geometry of 6 GHz cavity as compared to 1.3 GHz cavity combined with lack of suitable target material for both B1 and A15 superconductors and number of available cavities, similar success was not achieved up to now. The major obstacle is lack of suitable cylindrical target. Hence the only alternative is to use planar target with open cavity. For this reason, a split (open) 6 GHz cavity was designed and used in parallel at UKRI.

### 3.1.5 Split 6 GHz copper cavity

RF testing is essential to the advancement of superconducting cavities with thin film coatings. While significant progress has been made using flat samples, in order to gain a deeper understanding of the deposition process under realistic conditions it is necessary to test on RF cavities.

Traditionally, thin film copper cavities are produced in 2 half cells which are electron beam welded around their equator. Unfortunately, poor coating quality on the weld, as well as field enhancement can result in sub optimum cavity performance. A new cavity has been designed at Daresbury Laboratory which is produced as 2 longitudinally split cavity halves instead. This allows for a gap to be introduced, which the fields do not couple into, meaning the weld can be performed away from high field areas in the cavity.

In addition, the open faced design of the longitudinally split cavity allows for a greater number of deposition processes to be utilized and also allows for easier quality control of the cavity after deposition, both visually, and potentially using imaging equipment.

As a result, the new cavity design is being used at Daresbury for RF testing of thin film depositions. Initially, a simple 6 GHz cavity has been used for the testing, although in future a 1.3 GHz cavity, optimized specifically for use in an RF testing facility will be used.

Several tests have been performed with this cavity, primarily depositing with Niobium, and significant improvement has been seen as greater understanding of the deposition process, as well as cavity preparation processes have been gained.

## 3.2 SPLIT CAVITIES

### 3.2.1 Cavity Tests

Three Cavities have been produced at Daresbury Laboratory, machined from a solid copper block in two halves. The two halves are bolted together, and pins are used for alignment. The cavities (called Cavity A, B and C) are initially finished mechanically at Daresbury, and then two of them - cavity B and C - were sent to INFN/LNL to be electropolished, while cavity A remained behind, with only the mechanical finish from the machining process. These cavities were then deposited on via a sputtering process.

Once deposited, the cavities are tested inside a vacuum chamber, with a 2-plate system. An RDK-415D1 cold head is used to cool the system. The cavity is installed vertically to the second stage via copper plates, and a series of 4 heaters and 2 thermometers are attached directly to the cavity for heating and monitoring purposes.

The experiment goal is to measure the surface resistance ( $R_s$ ) of the cavities at a range of temperatures in order to gain insight into the quality of the deposition. Low surface resistance indicates minimal energy lost in the cavity walls, and therefore a better performing cavity. It can also be used to determine the critical temperature ( $T_c$ ) of the coating.

### 3.2.2 Results

One variable looked at was the temperature of the deposition. Cavity A was unpolished as shown in Fig. 24, meaning its rougher surface is likely to result in a higher surface resistance. The first test was Nb at room temperature, directly on top of copper, and then the following 2 films were deposited directly on top of this, at between 300 - 400 °C, the results are plotted on Fig. 25. Employing a higher deposition temperature led to reduced surface resistance during cavity testing. Specifically, room temperature measurements yielded surface resistances of  $532 \pm 10 \mu\Omega$  and  $393 \pm 6 \mu\Omega$ , whereas deposition at 300 – 400 °C resulted in a notably lower value of  $131 \pm 5 \mu\Omega$ . The difference between the depositions which used the same parameters can likely be attributed to improvements in the deposition process.



Figure 24. Two coated cavity halves, open for inspection prior to installation in the vacuum system.

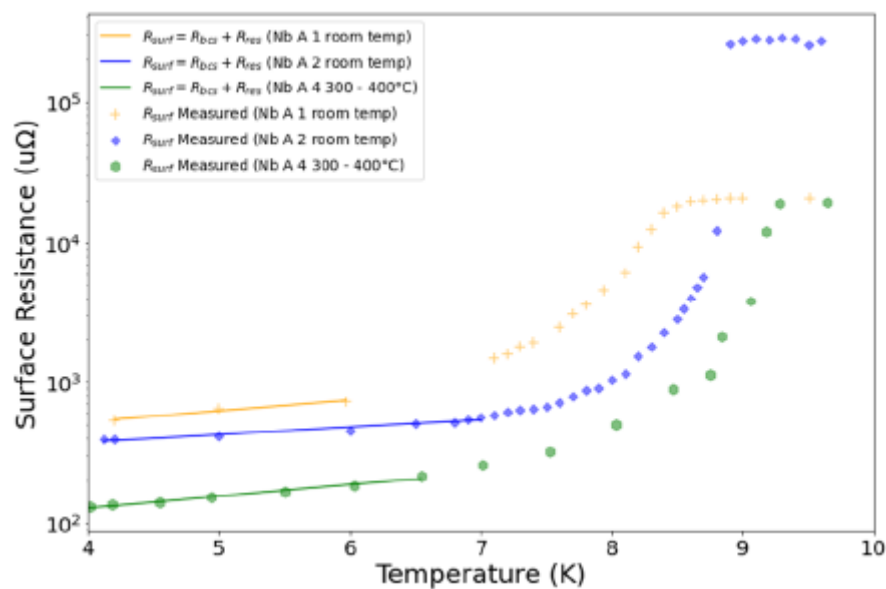


Figure 25. Different deposition temperatures have been compared using Cavity A - the mechanically finished cavity.

The substrate finish can have a significant effect on the overall result. In Fig. 26, it can be seen that with a smoother, electropolished finish a lower surface resistance was achieved. The cavities were deposited at temperatures ranging from 300 to 400 °C. The electropolished cavity had a surface resistance of  $55 \pm 3 \mu\Omega$ , while the mechanically finished cavity exhibited a value of 70  $\mu\Omega$  with 5  $\mu\Omega$ .

After these measurements, cavity A had its coating removed and was once again electropolished. It was deposited with Nb, at 300 - 400 °C, directly onto the copper, and performed better than any previously tested cavities, as shown in Fig. 27. It achieved a surface resistance at 4 K of 30  $\mu\Omega$  at 4K. The improved result is likely due to improvements in the deposition process as more cavities have been deposited.

In addition to Nb, a cavity has been deposited once for each of Nb<sub>3</sub>Sn and V<sub>3</sub>Si. The Nb<sub>3</sub>Sn cavity achieved  $153 \pm 4 \mu\Omega$ , and for the V<sub>3</sub>Si the cavity, the surface resistance at 4 K was  $300 \pm 10 \mu\Omega$ . These results are shown in Figs. 28 and 29 compared to the best performing Nb cavity. Currently, their performance has not been able to match that of niobium, however as only one deposition has been tested for each material, it is likely that further testing could see significant improvement. In addition, each of these depositions were performed on top of a previous niobium deposition. This was done in order to increase testing efficiency, but it is likely that this affected the results.

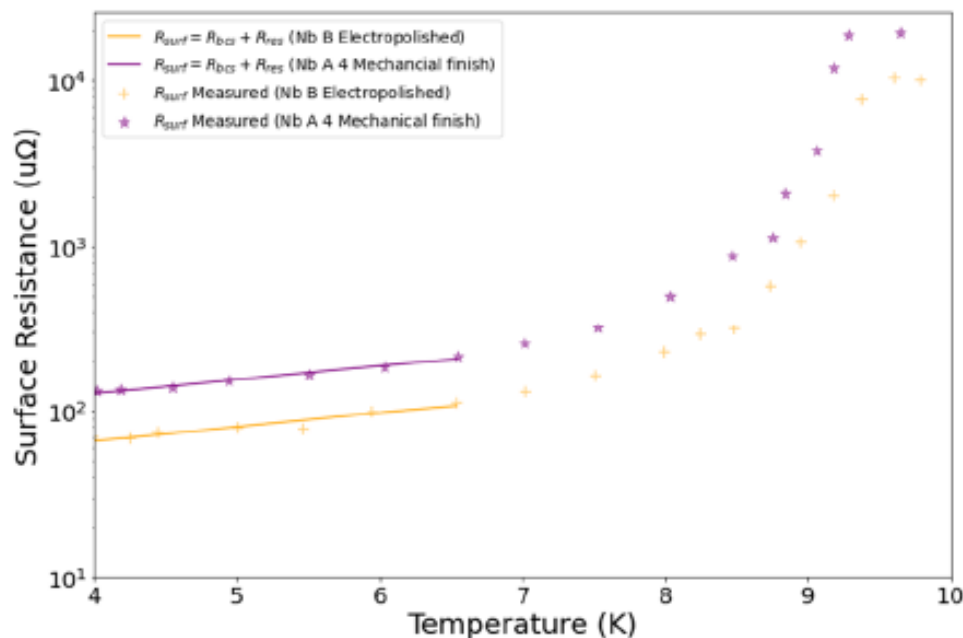


Figure 26. Looking at different cavity substrate finishes. With the same deposition parameters, Cavity B, which was electropolished performed better than Cavity A, which was only finished mechanically in the workshop.

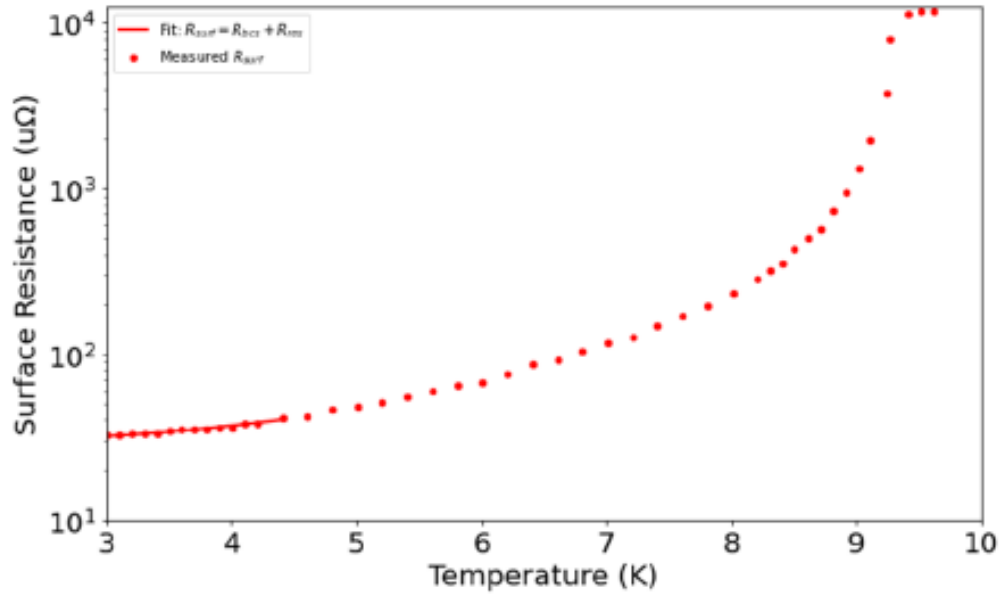


Figure 27.  $R_s$  against temperature for the best performing deposition. The split cavity was deposited with Nb on an electropolished substrate.

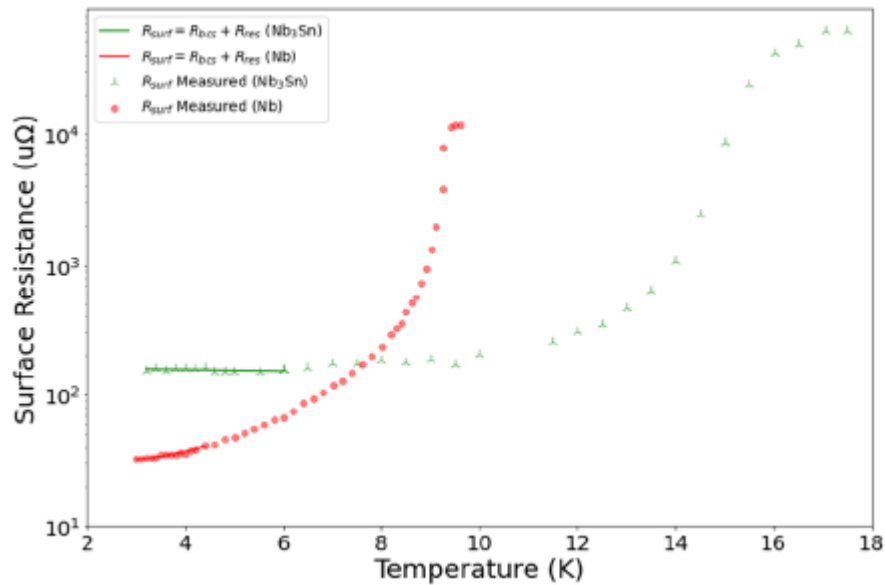


Figure 28. A  $Nb_3Sn$  film has also been tested, and plotted here alongside the highest performing Nb deposition.

Early simulations, from the beginning of the process of designing an optimized 1.3 GHz cavity showed that rounding the edge of the 6 GHz cavity should also improve results, due to minimizing peak fields that could be caused by misalignments in the cavity halves. As a result, cavity A had a 4 mm rounded edge added to each half.

This was then retested and Fig. 30 shows that the rounded cavity performed very well. Despite being unpolished, it achieved a surface resistance at 4 K of  $38 \mu\Omega$ , almost matching the results from the best polished cavity.

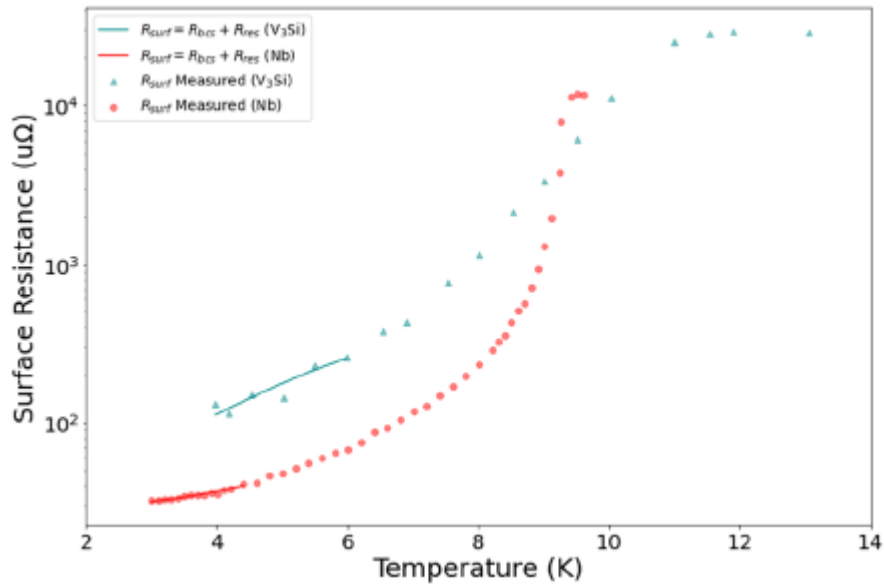


Figure 29.  $V_3Si$  plotted alongside the highest performing Nb results.

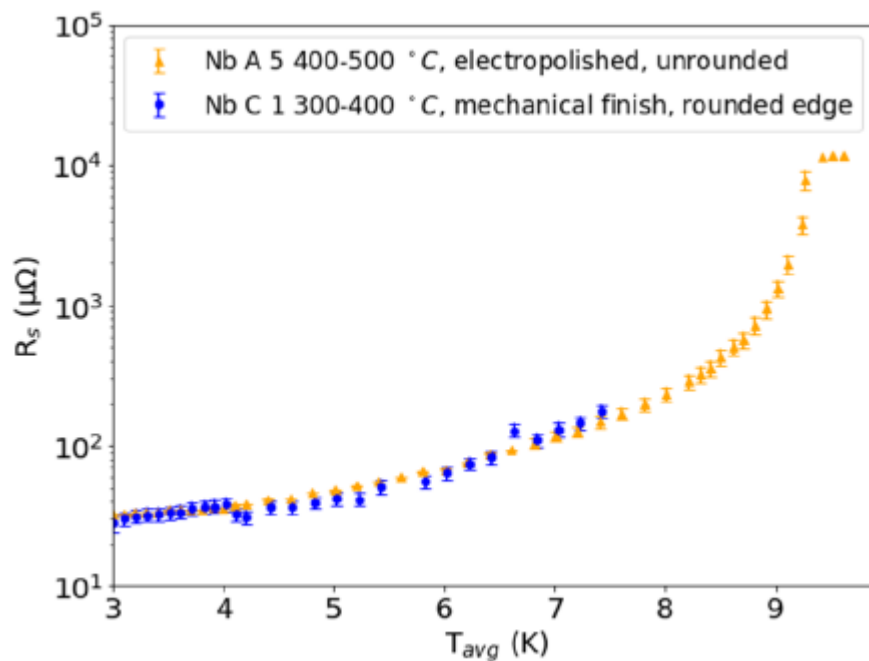


Figure 30. Two results for niobium films. The first shows the best results achieved on an unrounded cavity that has an electropolished substrate. The second shows the initial test of a rounded cavity, which was done on an unpolished substrate.

## 4 Target production at INFN

To enable coating of  $\text{Nb}_3\text{Sn}$  films in the 6 GHz system, it is necessary to replace the cylindrical Nb cathode with one of  $\text{Nb}_3\text{Sn}$  of the same geometry.

Conventional sintering from powders faces challenges in implementing the required features for cooling the cylindrical cathode due to material fragility. An alternative approach involves producing targets through the growth of thick films of  $\text{Nb}_3\text{Sn}$  directly on a niobium substrate using the Liquid Tin Diffusion (LTD) technique has been explored at INFN as depicted in Fig. 31.

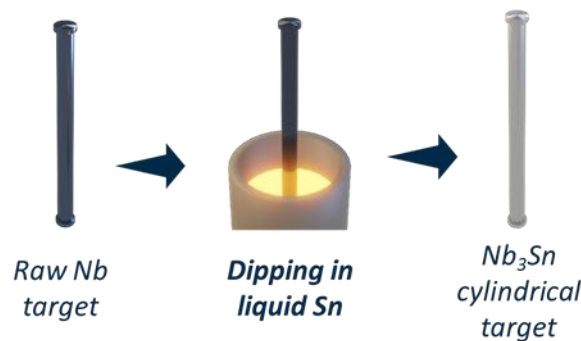


Figure 31. Pictorial sequence of  $\text{Nb}_3\text{Sn}$  target production by dipping technology.

### 4.1 PROOF OF CONCEPT ON OLD DIPPING SYSTEM

In INFN-LNL a dipping system has been designed and built in 2005 for the coating 6 GHz elliptical cavities. The set-up consists of an alumina crucible that contains molten tin on which the Nb sample is immersed. 2 resistive furnaces are used to heat the tin contained in the crucible and to anneal the sample after immersion in the tin and promote the growth of  $\text{Nb}_3\text{Sn}$ , respectively as shown in Fig. 32. The operating temperatures are 1000 °C.

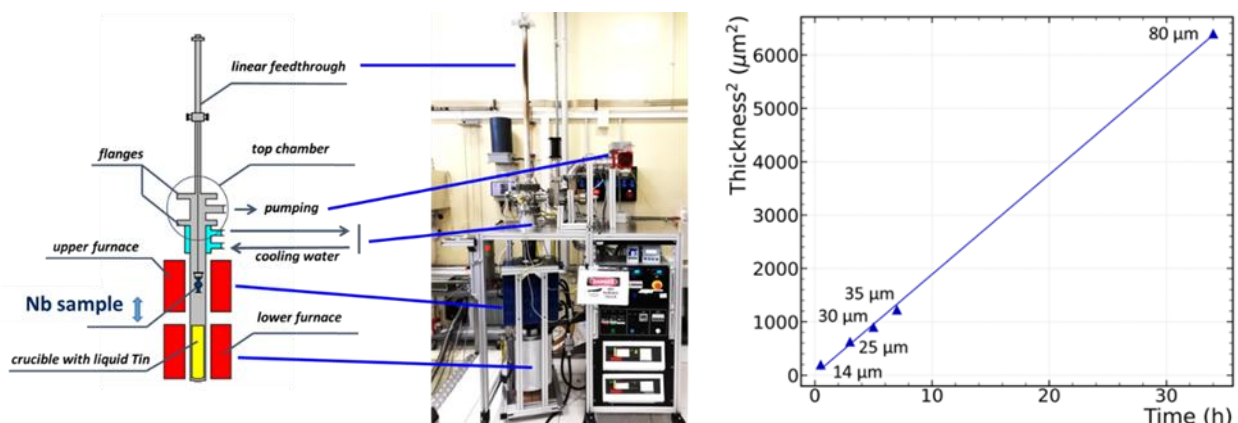


Figure 32. On the left: the old dipping facility at INFN. Two resistive furnaces were used to heat up to 1000 °C the Inconel vacuum chamber. On the right: a direct correlation has been found between dipping time and the square of  $\text{Nb}_3\text{Sn}$  thickness.



Prior to the start of I.FAST, a successful proof of concept was done on 1" planar targets, which demonstrated the feasibility of growing 35  $\mu\text{m}$  of  $\text{Nb}_3\text{Sn}$  via dipping on an Nb disk and sputtering it for more than 6 microns, obtaining a stoichiometric coating.

During I.FAST, the study was continued, demonstrating the feasibility of growing up to 80  $\mu\text{m}$  and confirming that the growth thickness is proportional to the square root of the dipping time. In addition, the growth process was optimized, inspired by the vapor tin diffusion process. The Nb substrate is electrochemically anodized, and an initial nucleation step was added to the deposition protocol (Fig. 33).

These optimizations reduced the main problem of the process, which was the formation of tin-rich clusters on the surface, allowing the growth of a uniform, stoichiometric film. However, the high quality of the coatings revealed an unknown problem, which was chromium contamination on the surface. Small contaminations of chromium are extremely harmful in SRF cavities and should therefore be eliminated. The source of contamination was recognized in the inconel vacuum chamber and therefore it was decided to replace it with a bulk Nb vacuum chamber manufactured in Zanon.

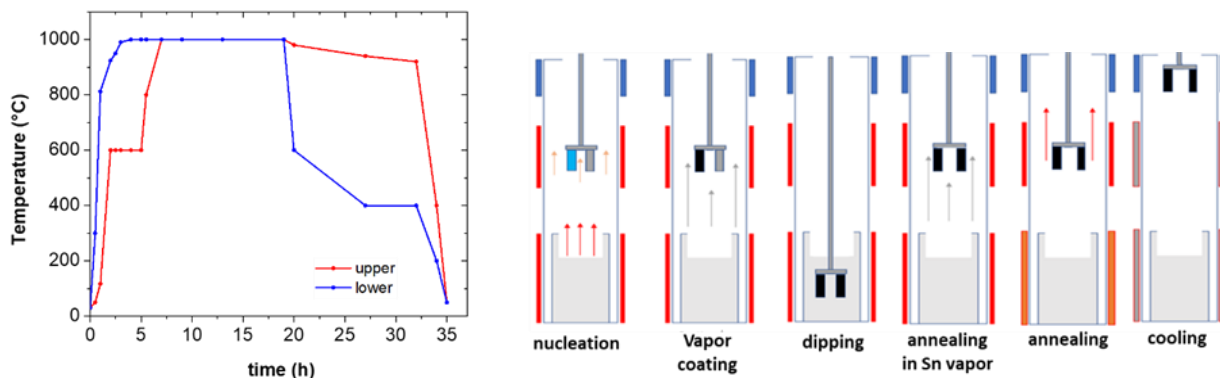


Figure 33. The new dipping protocol developed in IFAST.

## 4.2 NEW DIPPING SYSTEM

The necessity of using an Nb chamber to prevent Cr contamination, however, completely overturned the project's initial development plans, causing a quantifiable delay of more than 2 years on the production of the  $\text{Nb}_3\text{Sn}$  cylindrical targets.

In particular, the use of an Nb chamber, in fact, required a complete re-design of the system set-up [24]. It was no longer possible to work with resistive heating in air, but had to switch to inductive heating in a vacuum to prevent oxidation of the outer walls of the Nb chamber. A system with a double vacuum was then implemented with the design and commissioning of a new large SS vacuum chamber capable to contain the Nb chamber (see Fig. 34). The new chamber features a front-opening door for inspection and multiple CF flanges to allow for enhanced flexibility and future upgrades capability. The chamber is designed to be fully water-cooled and will be mounted on a mobile and modular system.

Regarding the heating process, a new custom-made induction heating system has been designed, commissioned and implemented. This system enables complete control of the process parameters via a computer interface, including the option for remote control and monitoring. The induction heating system has been configured to address the specific requirements of heating two distinct zones within the chamber independently, ensuring the execution of various process steps. Simulations have been conducted to size and optimize the induction heating system. Power levels of 1800W and 1700W have been selected for the upper and lower coils, respectively. Each inductor consists of 20 turns. This configuration ensures the attainment of selective heating in two different zones of the chamber.

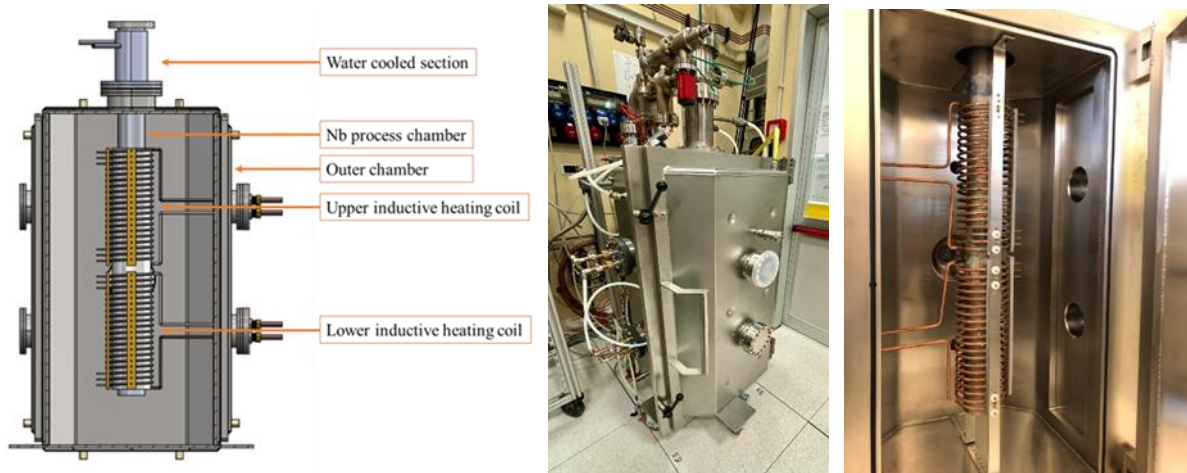


Figure 34. The new inductive dipping system installed in INFN.

The target temperature for the new system is 1100 °C, given by the Nb-Sn phase diagram. Indeed, at this temperature it is possible to avoid the formation of spurious phases and form only the stoichiometrically correct A15 phase. Commissioning was completed in March 2024, but at present the inductive system cannot reach the target temperature, limited to 600 °C by a design error of the manufacturing company (see Fig. 35), which is currently working on the solution.

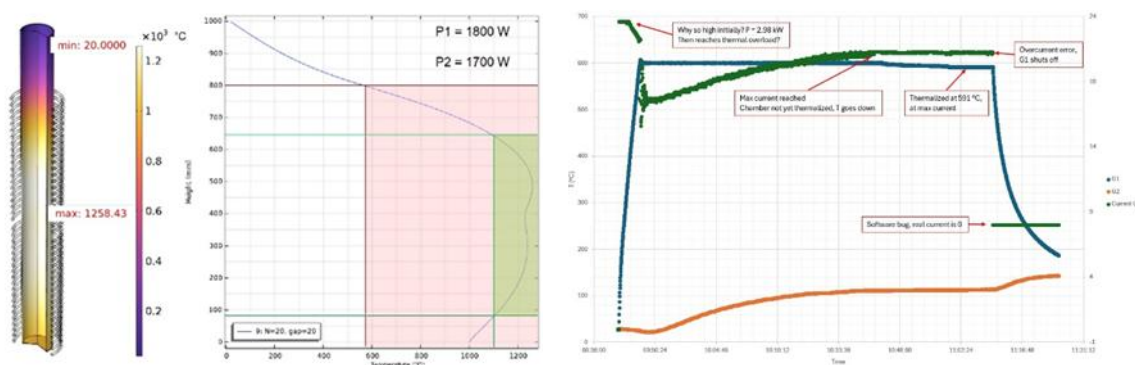


Figure 35. On the left: simulation of Nb chamber operational temperature. On the right: Measured operational temperature.

We expect that the inductive system will be fixed by the end of 2025, and we can then proceed with the development and production of Nb<sub>3</sub>Sn targets, which are critical for coating Nb<sub>3</sub>Sn within the 6 GHz cavities.

## 5 Conclusions and relation to other IFAST work

### 5.1 MAIN RESULTS

A total of 3 seamless 6 GHz cavities and 4 split 6 GHz cavities has been coated and characterized fulfilling the original deliverable.

On top of that, a deep R&D has been done in Task 9.3, exploring different superconductors materials and different coating techniques, to provide a pathway to the main WP9 deliverable in Task 9.2: coating technology for 1.3 GHz cavity.

Starting from the results obtained by UKRI in ARIES, two parallel studies conducted by UKRI and INFN in I.FAST thoroughly investigated the effect of deposition parameters on the properties of Nb<sub>3</sub>Sn, with the aim of maximizing its  $T_c$  and thus minimizing the surface resistance ( $R_s$ ) of SC coatings. The main results are the following:

- Nb<sub>3</sub>Sn seems to be more suitable candidate for operation at  $T = 4$  K as lower  $R_s$  than NbTiN has been obtained.
- Nb<sub>3</sub>Sn deposition parameters set by UKRI during ARIES program without any post annealing gives the best results for both films deposited at UKRI and INFN. This recipe should be tweaked for each deposition facility to produce the optimum results.
- Optimum deposition power density for Nb<sub>3</sub>Sn is established with values in DC Power  $< 3$  W/cm<sup>2</sup>.
- Optimum deposition temperature for Nb<sub>3</sub>Sn on Cu and Nb is at 570 and 650 °C respectively.
- Films on Cu and Nb buffer layer substrate of 30 μm with a  $T_c \geq 17$  K and an RF surface resistance of 23 nΩ at 4.5 K, 20 mT and 400 MHz.
- Choke cavity, 6 GHz cavity (open and closed) and QPR are crucial methods for optimization of SRF properties of the thin film.
- For target production by Nb dipping in molten Sn, Inconel furnace chamber is detrimental and results in inclusion of Cr as impurity.

Troubles met during this task:

- Lack of suitable cylindrical targets available on a market for high  $T_c$  superconductor A15 and B1 is the major problem for PVD deposition of RF cavity.

### 5.2 FUTURE PLANS

Due to success achieved in IFAST, the future plan is most likely to concentrate on deposition of 1.3 GHz cavities made of both Nb and Cu. The planar studies will be concentrated on the employment

of both A15 and B1 as SIS structures. The main difficulty was lack of suitable target for 3D geometry; considerable effort will be assigned to address this problem.

## 6 References

---

- [1] Gurevich, A., "Enhancement of RF breakdown field of superconductors by multilayer coating". Appl. Phys. Lett. 88, p. 012511A (2006).
- [2] P. Dhakal *et al*, Phys. Rev. Spec. Topics Accel. Beams **16**, 042001 (2013).
- [3] A. Grassellino *et al*, Supercond. Sci. Technol. **26**, 102001 (2013).
- [4] G. Ciovati, P. Dakhal and A. Gurevich, Appl. Phys. Lett. **104**, 092601 (2014).
- [5] V. Palmieri, 10<sup>th</sup> Workshop on RF Superconductivity Proc. (Tsukuba, Noguchi), p. 162 (2001).

### List of Task 9.3 publications

#### NbTiN papers:

- [6] S. Simon, C. Benjamin, J. Bradley, R. Valizadeh Comparison on the superconducting properties of Nb and NbTiN thin films produced by both HiPIMS and bipolar HiPIMS. In Proc. of IPAC'2024, Nashville, USA, 19-24 May 2024, p. 2802, paper WEPS48.

#### V<sub>3</sub>Si papers:

- [7] C. Benjamin, R. Valizadeh, L. Smith, O.B. Malyshev, J. Conlon, E. Seiler, R. Ries, G. Stenning, V<sub>3</sub>Si thin films for SRF applications. In Proc. of IPAC'23, Venice, Italy, 07-12 May 2023, p. 3071, paper WEPA184.
- [8] T. Sian, J. Conlon, O.B. Malyshev, R. Valizadeh, G. Burt, N. Leicester, H. Marks, C. Pira, E. Chyhyrnyets. V<sub>3</sub>Si thin films for SRF applications. In Proc. of IPAC'23, Venice, Italy, 07-12 May 2023, p. 3074, paper WEPA185.
- [9] C. Benjamin, L. Smith, J.A. Conlon, O.B. Malyshev, R. Valizadeh, D. Seal, N. Leicester, H. Marks, G. Burt. Deposition and characterisation of V<sub>3</sub>Si films for SRF applications. In Proc. of SRF2023, Grand Rapids, USA, 25-30 June 2023, p. 84, paper MOPMB011.
- [10] C. Benjamin, D. Seal, G. Stenning, J. Conlon, O.B. Malyshev, R. Valizadeh. V<sub>3</sub>Si: an alternative thin film material for superconducting RF cavities. In Proc. of IPAC'2024, Nashville, USA, 19-24 May 2024, p. 2779, paper WEPS39.

**SIS papers:**

[11] A.Ö. Sezgin, X. Jiang, M. Vogel, R. Ries, E. Seiler, D. Tikhonov, S. Keckert, J. Knobloch, O. Kugeler, L. Smith, O. B. Malyshev, C. Z. Antoine. Investigation of HiPIMS-Coated S(I)S Structures for SRF Cavities. In Proc. LINAC2022, Liverpool, UK, 28 August - 2 September 2022, p. 805 (2022).

**T<sub>c</sub> and magnetic field penetration papers:**

[12] L. Smith, D. Turner, G. Burt, T. Junginger, O.B. Malyshev. Investigation, using Nb foils to characterise the optimal dimensions of samples measured by the magnetic field penetration facility. In Proc. of SRF2023, Grand Rapids, USA, 25-30 June 2023, p. 88, paper MOPMB012.

[13] D. Seal, C. Benjamin, O. Malyshev, K. Sian, L. Smith, R. Valizadeh, J. Wilson. G. Burt<sup>1</sup>, N. Leicester. Upgraded multiprobe sample inserts for thin film SRF cavity developments. In Proc. of IPAC'2024, Nashville, USA, 19-24 May 2024, p. 2960, paper WEPS38.

**7.8 GHz cavity papers:**

[14] D. Turner, O.B. Malyshev, G. Burt, T. Junginger, R. Valizadeh, L. Gurran. A facility for the characterisation of planar multilayer structures with preliminary Niobium results. Supercond. Sci. Technol. 35, 095004 (2022).

[15] D.A. Turner, O.B. Malyshev, G. Burt, E. Seiler, R. Ries, A. Medvids, P. Onufrijevs, R. Valizadeh, A. Sublet, C. Pira, E. Chyhyrynets, M. Vogel, S. Leith, T. Junginger. Investigating the Superconducting Properties and Surface Morphology of Sputtered Nb Films on Cu Due to Laser Treatment. IEEE Transactions on Applied Superconductivity 33 (4), 7500512 (2023).

[16] D. Seal, O.B. Malyshev, P. Goudket, T. Sian, L. Gurran, R. Valizadeh, H. Marks, S. Pattalwar, N. Pattalwar, C. Pira, E. Chyhyrynets and G. Burt. A high throughput facility for the RF characterisation of planar superconducting thin films. Superconductor Science and Technology, (2024).

[17] D. Seal, O.B. Malyshev, R. Valizadeh, T. Sian, H. Marks, O. Hryhorenko, D. Longuevergne, C. Pira, E. Chyhyrynets, E. Marshall, G. Burt. RF Characterisation of Bulk Niobium and Thin Film Coated Planar Samples at 7.8 GHz. In Proc. LINAC2022, Liverpool, UK, 28 August – 2 September 2022, p. 818 (2022).

[18] D. Seal, G. Burt, J. Conlon, O.B. Malyshev, K. Morrow, R. Valizadeh. Optimisation of niobium thin film deposition parameters for SRF cavities. In Proc. of SRF2023, Grand Rapids, USA, 25-30 June 2023, p. 253, paper MOPMB062.

**6 GHz cavity papers:**

[19] R. Valizadeh, A.N. Hannah, O.B. Malyshev, V.R. Dhanak, G. Stenning, E. Chyhyrynets, V.A. Garcia Diaz, C. Pira. A first 6 GHz cavity deposition with B1 superconducting thin film at ASTeC. In Proc. IPAC'22, Bangkok, Thailand, 12-17 June 2022, p. 1279 (2022).

### **Split cavity papers:**

[20] T. Sian, G. Burt, D. Seal, H. Marks, R. Valizadeh, O.B. Malyshev. Split Thin Film SRF 6 GHz Cavities. In Proc. LINAC2022, Liverpool, UK, 28 August - 2 September 2022, p. 814 (2022).

[21] N.L. Leicester, G. Burt, H.S. Marks, D. Seal, J. Conlon, O.B. Malyshev, T. Sian, R. Valizadeh. Development and testing of split 6 GHz cavities with niobium coatings. In Proc. of SRF2023, Grand Rapids, USA, 25-30 June 2023, p. 51, paper MOPMB001.

### **Nb<sub>3</sub>Sn papers:**

[22] D. Fonnesu et al., “Influence of the Coating Parameters on the T<sub>c</sub> of Nb<sub>3</sub>Sn Thin Films on Copper Deposited via DC Magnetron Sputtering”, in Proc. 21th Int. Conf. RF Supercond. (SRF'23), Grand Rapids, MI, USA, Jun. 2023, pp. 92-95. doi:10.18429/JACoW-SRF2023-MOPMB013

[23] C. Pira et al., “Progress in European Thin Film Activities”, in Proc. 21th Int. Conf. RF Supercond. (SRF'23), Grand Rapids, MI, USA, Jun. 2023, pp. 607-614. doi:10.18429/JACoW-SRF2023-WECAA01

[24] D. Ford et al., “Study and Improvements of Liquid Tin Diffusion Process to Synthesize Nb<sub>3</sub>Sn Cylindrical Targets”, in Proc. 21th Int. Conf. RF Supercond. (SRF'23), Grand Rapids, MI, USA, Jun. 2023, pp. 868-871. doi:10.18429/JACoW-SRF2023-WEPWB118

Several abstracts with results presented in this report have been submitted to and the talk will be presented at the SRF2025 conference that will take place in Tokyo on 25-26 Sep 2025.